

Stochastic optimization algorithms for quantum applications

J. A. Gidi,^{1,*} B. Candia,^{1,2} A. D. Muñoz-Moller,^{1,2} A. Rojas,^{1,2} L. Pereira,³ M. Muñoz,^{4,5} L. Zambrano,^{1,2} and A. Delgado^{1,2}

¹*Departamento de Física, Facultad de Ciencias Físicas y Matemáticas,
Universidad de Concepción, Casilla 160-C, Concepción, Chile*

²*Instituto Milenio de Investigación en Óptica, Universidad de Concepción, Concepción, Chile*

³*Instituto de Física Fundamental IFF-CSIC, Calle Serrano 113b, Madrid 28006, Spain*

⁴*Departamento de Ingeniería Matemática, Facultad de Ciencias Físicas y Matemáticas,
Universidad de Concepción, Casilla 160-C, Concepción, Chile*

⁵*Centro de Investigación en Ingeniería Matemática (CIM2MA),
Universidad de Concepción, Casilla 160-C, Concepción, Chile*

Hybrid classical quantum optimization methods have become an important tool for efficiently solving problems in the current generation of NISQ computers. These methods use an optimization algorithm that is executed in a classical computer, which is fed with values of the objective function that are obtained in a quantum computer. Therefore, a proper choice of optimization algorithm is essential to achieve good performance. Here, we review the use of first-order, second-order, and quantum natural gradient stochastic optimization methods, which are defined in the field of real numbers, and propose new stochastic algorithms defined in the field of complex numbers. The performance of the methods is evaluated by means of their application to variational quantum eigensolver, quantum control of quantum states, and quantum state estimation. In general, complex number optimization algorithms perform better and second-order algorithms provide a large improvement over first-order methods in the case of variational quantum eigensolver.

I. INTRODUCTION

The current generation of quantum hardware has been described as noisy intermediate scale quantum devices (NISQ) [1], which are characterized by noisy entangling gates, short coherence times, and large sampling error. A promising approach to achieve quantum advantage in NISQ devices is hybrid quantum-classical optimization algorithms [2–5]. These use a quantum algorithm to evaluate an objective function through a parameterized quantum circuit in a quantum computer, while the values of the objective function are inputs to a classical optimization algorithm running on a classical computer. Thus, hybrid optimization algorithms are used whenever the objective function can be evaluated more efficiently on a quantum computer than on a classical one. This is the case for applications to quantum chemistry [6–8], quantum control [9–11], quantum simulation [12, 13], entanglement detection [14–16], state estimation [17–21], quantum machine learning [22–26], error correction [27], graph theory [28–30], differential equations [31–33], and finances [34].

The performance of hybrid quantum-classical optimization is affected by the optimization landscape associated with the objective function and the choice of optimization algorithm. For instance, it has been recently shown [35, 36] that a very general class of objective functions exhibit a barren plateau, that is, a region in the optimization landscape where the objective function gradient vanishes exponentially with the number of qubits. In particular, this affects applications where random quantum circuits are used, such as, for instance, quantum machine learning [23]. Also recently, several studies [37–40] have been carried out to establish general guidelines to

choose the optimization algorithm with the best performance, according to a predefined metric, for a certain class of problems. These consider methods such as Stochastic Gradient Descent [41], Adaptive Gradient Algorithm [42], Root Mean Square Propagation [43], Adam and variations [44–46], Nelder-Mead [47], Powell method [48], and Newton Conjugate Gradient [49], among many others [50–56].

Among the growing list of methods applied to hybrid optimization, stochastic optimization algorithms [57–61] play an important role. State initialization, quantum gates, and measurements are noisy processes that lead to noisy evaluations of the objective function. This intrinsically stochastic behaviour of the objective function negates mathematical guarantees on convergence of commonly used classical optimization methods [39]. However, certain stochastic optimization methods have convergence proofs that admit the presence of noise. In this scenario, a method that achieves good performance in several applications to hybrid optimization is the simultaneous perturbation stochastic approximation (SPSA) method [62]. The main advantages of SPSA are their robustness to noise, which is ubiquitous in quantum mechanics, and that it can approximate the gradient of an objective function with only two measurements of the objective function. In particular, this approximation does not require knowing the operational form of the objective function. SPSA has been successfully implemented in several experimental platforms and is one of the standards methods for training variational quantum eigensolvers (VQEs) [63–67], quantum neural networks (QNNs) [68–70], and quantum tomography [17, 18, 71].

Given the success of the Stochastic Optimization algorithms within quantum computing, there have been efforts to improve their performance in solving certain tasks. One proposal is the second-order SPSA (2SPSA), which uses the inverse of a simultaneous perturbation estimate of the Hessian of the objective function to precondition the gradient in order to improve the convergence rate [72, 73]. This method is

* jorgegidi@udec.cl

inspired by the deterministic Newton-Raphson algorithm and requires four evaluations of the objective function per iteration to estimate both gradient and Hessian. It has been shown that this method achieves a nearly optimal asymptotic error for well-conditioned problems, but the error is several orders of magnitude higher when the Hessian is ill-conditioned [74]. Given that, it is not clear when the 2SPSA algorithm provides an advantage over the SPSA algorithm. Another proposal focused on quantum computing is quantum natural gradient optimization [75]. The SPSA algorithm explores the parameter space within a flat geometry, which can cause the parameters to be updated inappropriately. In contrast, quantum natural gradient uses information about the geometry of the parametric quantum state to update the parameters appropriately. This information is represented by the Fubiny-Study metric tensor. Natural gradient optimization provides several advantages over vanilla methods because this is invariant under re-parametrizations [76] and approximate invariant under over-parametrizations [77]. The quantum natural approach of SPSA (QN-SPSA) is based on a simultaneous perturbation estimate of the Fubiny-Study metric tensor [78]. This estimation requires four evaluations of fidelity per iteration in addition to the two function evaluations for the gradient. The fidelity evaluation can be performed efficiently using the swap-test [79], among others alternatives [80]. This method is appropriate in contexts where the evaluation of the objective function is too expensive, for example, in the estimation of the fundamental energy of molecules. [65, 66, 81, 82]. However, similarly to 2SPSA, ill-conditioned metrics can reduce the performance of the algorithm [83–85].

Optimization methods can be also extended to work in the field of complex numbers by the means of Wirtinger calculus [86]. Some examples are the complex Newton-Raphson algorithm [87] and the complex quantum natural gradient [88]. These methods optimize the objective function without resorting to the real and imaginary parts of complex variables. It has been argued in the literature that optimization methods formulated within the complex numbers could achieve better performance, which has been observed in a small set of examples [89–91]. Moreover, this is a more natural approach to work in the field of quantum mechanics, where most functions have complex arguments. For example, continuous variable quantum computation employs displacement and squeeze operations, which depend on complex parameters [92, 93]. Recently, the complex simultaneous perturbation stochastic approximation (CSPSA) method [19] has been introduced. This is a generalization of SPSA that works optimizing complex parameters. It has been shown that CSPSA can deliver better results in the estimation of pure states [19] and that it is robust against noise [21]. It has been applied to entanglement estimation [16] and quantum state discrimination [26].

Here, we present a comparative analysis of several stochastic optimization methods applied to real-valued functions of complex variables. We first review the basic principles of the SPSA algorithm. Subsequently, we review the 2SPSA and QN-SPSA algorithms, which are built using SPSA as a guideline. We also review the CSPSA algorithm, and moreover, we developed two new optimization algorithms building upon the

CSPSA algorithm: 2CSPSA and QN-CSPSA. These are the complex field formulations of their real counterparts 2SPSA and QN-SPSA, respectively. We study the performance of the introduced methods by comparing their rate of convergence, as a function of the number of evaluations (or measurements) of the objective function or quantum circuits, with respect to SPSA, 2SPSA and QN-SPSA. This comparison is carried out in three important applications in quantum computing: variational quantum eigensolver, quantum control, and quantum state estimation. We use a variational quantum eigensolver to obtain the ground state energy of the Heisenberg Hamiltonian, which is an ubiquitous and relatively simple model that describes the interactions within a chain of spins [63]. We implement the Gradient Ascent Pulse Engineering (GRAPE) method [94], which is used to engineer quantum gates and states. This method approximates a control pulse by a sequence of constant intensity pulses. The control parameters of this pulse are optimized in order to find the best implementation of a given gate or state, even in the presence of noise [9]. Finally, in quantum state estimation we implement Self-Guided Quantum Tomography (SGQT) [17], which is based on the minimization of the infidelity between an unknown state and a known parametrized state. Since the studied optimization methods are stochastic in nature we use numerical simulations and estimate mean, variance (or standard deviation), median, and interquartile range. Measurements are simulated using a finite sample of various sizes.

Our comparative analysis shows that overall complex-based optimization methods leads to better performance than real-based optimization methods. In particular, CSPSA exhibits a better performance than SPSA not only in the case of state estimation but also in variational quantum eigensolver and quantum control. This is specially clear in the case of VQE, where CSPSA achieves a convergence toward the minimum with a much smaller number of circuits than SPSA. Furthermore, CSPSA exhibits a narrower interquartile range than SPSA. In the case of quantum control, the infidelity as a function of the number of evaluations or measurements of the objective function shows a step decrease followed by an asymptotic linear behavior. In the latter regime, CSPSA requires approximately half the number of function evaluations than SPSA to achieve a similar value of the infidelity. An analogous phenomenon can be observed in the case of state estimation. The performance of the second-order methods 2SPSA and 2CSPSA depends on the particular application. In the case of VQE, 2CSPSA and 2SPSA achieve an almost equal performance and provide a clear advantage over CSPSA, SPSA, QN-CSPSA and QN-SPSA. In quantum control, CSPSA outperforms all other algorithms.

This article is organized as follows: in Section II we review the stochastic optimization methods SPSA, 2SPSA, QN-SPSA and CSPSA and formulate the methods 2CSPSA and QN-CSPSA. In Section III we apply the previously developed optimization methods to variational quantum eigensolver, quantum control, and quantum state estimation. In section IV we summarize our main results and conclude.

II. STOCHASTIC OPTIMIZATION ALGORITHMS

Consider the optimization problem of a real function of p complex variables, $f : \mathbb{C}^p \rightarrow \mathbb{R}$, that is, finding some argument $z^* \in \mathbb{C}^p$ such that $f(z^*)$ is a local minimum of the function f . This problem can be solved by mapping the complex variables to the field of the real numbers through the relation $z = \mathbf{x} + i\mathbf{y}$, in which case now f becomes $f(\boldsymbol{\theta})$ with $\boldsymbol{\theta} = (\mathbf{x}, \mathbf{y})^T \in \mathbb{R}^{2p}$. Then, one can use real-variable optimizers to find $\boldsymbol{\theta}^* = (\mathbf{x}^*, \mathbf{y}^*)^T$ such that $f(\boldsymbol{\theta}^*)$ is a minimum of f , and recover the solution for the original complex-variable problem as $z^* = \mathbf{x}^* + i\mathbf{y}^*$. It is possible, nevertheless, to solve the optimization problem using Wirtinger calculus [86, 95], which does not resort to mapping the complex variables to the real numbers.

While both of this approaches are equivalent, the process of solving one or another is not. It has been conjectured that a complex-variable reformulation of real-variable optimization algorithms may lead to a performance boost [89–91], which has been observed when working on pure-state quantum tomography [19]. Furthermore, for quantum applications, which are natively posed in terms of complex variables, the transformation to real variables adds an extra complexity step in the resolution and poses the problem in an unnatural way, being potentially detrimental to the understanding of the phenomena in question. For this reason, here we will review some real-variable optimization methods relevant for quantum applications, and then we will present their analog complex-variable reformulation.

A specially well suited class of methods for optimizing a multivariate function in the presence of noisy measurements are the stochastic approximation methods [57–61]. This family of methods originates from the Robbins-Monro algorithm [96] designed to find a root θ of a function $M(\mathbf{x})$ given by the expectation of a random variable $Y(\mathbf{x})$. Here M has unknown nature as well as the probability function of Y , and the Robbins-Monro algorithm delivers an estimate of θ by making successive observations on Y . From the Robbins-Monro algorithm it is possible to consider M as a regression function [97] and propose a scheme to estimate the maximum of M . Thereby, a very especial use of stochastic approximations arises to deliver an algorithm that converges to an optimal value of a function f using the Kiefer and Wolfowitz procedure when $M = \nabla f$.

A widely used family of stochastic approximation (SA) methods rely on the iterative rule

$$\boldsymbol{\theta}_{k+1} = \boldsymbol{\theta}_k - a_k \mathbf{g}_k(\boldsymbol{\theta}_k), \quad (1)$$

where the descent step series, $a_k = a/(k + A)^s$, is fixed by the externally selected gain parameters a , A and s . Also, \mathbf{g}_k is some stochastic approximation to the gradient of the objective function at $\boldsymbol{\theta}_k$, which depends on a gain coefficient $b_k = b/k^t$, where b and t also are externally fixed gain parameters. While choosing a good set $\{a, b, A, s, t\}$ of gain parameters is very relevant for the adequate performance of the optimization methods, they will only be mentioned briefly as this, an optimization problem itself, lies out of the scope of this article.

In the following we review the stochastic approximations used by the SPSA algorithm and its extensions to the second-order algorithm 2SPSA and quantum natural gradient algorithm QN-SPSA. Subsequently, we extend the iterative rule Eq. (1) to the case of complex variables, review the CSPSA algorithm, and develop its extensions to the second-order algorithm 2CSPSA and quantum natural gradient algorithm QN-CSPSA. This is done following a similar approach to SPSA.

A. Real-variable methods

1. SPSA

The simultaneous perturbation stochastic approximation (SPSA) is a multivariate optimization method for real functions of real variables. While the SPSA denomination came later, the method was first presented by Spall [62] and corresponds to an improvement over the finite difference stochastic approximation (FDSA) from Kiefer and Wolfowitz [97]. Both the FDSA and SPSA algorithms optimize the function $f(\boldsymbol{\theta})$ with $\boldsymbol{\theta} \in \mathbb{R}^p$, at iteration k , by following the recursive stochastic approximation rule (1). However, the main feature of SPSA is that, instead of estimating each of the p components of the gradient as a stochastic finite difference approximation as the FDSA method does, it defines the estimator \mathbf{g}_k as

$$\mathbf{g}_k(\boldsymbol{\theta}) = \frac{f(\boldsymbol{\theta} + b_k \boldsymbol{\Delta}_k) - f(\boldsymbol{\theta} - b_k \boldsymbol{\Delta}_k)}{2b_k} \begin{pmatrix} 1/\Delta_{k,1} \\ \vdots \\ 1/\Delta_{k,p} \end{pmatrix}, \quad (2)$$

where $\boldsymbol{\Delta}_k$ is a random perturbation vector with p components uniformly generated from the set $\{\pm 1\}$, and the finite-difference approximation step $b_k = b/k^t$ is controlled by the externally selected gain parameters b and t . It is worth noting that while $\mathbf{g}_k(\boldsymbol{\theta}_k)$ does not necessarily have the direction of the gradient at each iteration, it is an asymptotically unbiased estimator of the same, which means that it converge in the statistical limit to the same solution as following the gradient. Also, definition (2) makes the SPSA algorithm specially suitable for high-dimensional problems, since it always requires 2 function evaluations per iteration, independent of the number of variables, p , in contrast to the FDSA algorithm that requires $2p$ function evaluations per iteration.

An iteration of the SPSA algorithm is given by Eqs. (2) and (1).

2. 2SPSA

Noting that the iterative rule used in the SPSA algorithm follows from a first-order gradient descent approximation to move towards the optimal value $\boldsymbol{\theta}^*$, one could accelerate the convergence rate of the method by using a second-order iterative rule coming from the Newton-Raphson algorithm

$$\boldsymbol{\theta}_{k+1} = \boldsymbol{\theta}_k - \eta [\mathcal{H}(\boldsymbol{\theta}_k)]^{-1} \left(\frac{\partial f}{\partial \boldsymbol{\theta}}(\boldsymbol{\theta}_k) \right)^T, \quad (3)$$

where $\eta \in \mathbb{R}^+$ is the learning rate and \mathcal{H} is the Hessian of f . A stochastic approximation based on Eq. (3) is proposed by Spall [72], deriving the so-called adaptative or second-order SPSA (2SPSA) algorithm. The iterative rule now yields

$$\boldsymbol{\theta}_{k+1} = \boldsymbol{\theta}_k - \bar{a}_k \bar{\mathcal{H}}_k^{-1} \mathbf{g}_k(\boldsymbol{\theta}_k), \quad (4)$$

where $\bar{a}_k = 1/(k+A)^s$ no longer depends on a . The gradient estimator \mathbf{g}_k is defined by Eq. (2) as in the first-order case, and $\bar{\mathcal{H}}_k$ is a modified version of the simultaneous perturbation stochastic approximation of the Hessian matrix. In particular, based on recommendations from Spall [72] and our numerical experiments, we compute $\bar{\mathcal{H}}_k$ by

$$\bar{\mathcal{H}}_k = \frac{k}{k+1} \bar{\mathcal{H}}_{k-1} + \frac{1}{k+1} \mathcal{H}_k'' \quad (5a)$$

$$\mathcal{H}_k'' = \sqrt{\mathcal{H}_k'^2 + \varepsilon I} \quad (5b)$$

$$\mathcal{H}_k' = \frac{\mathcal{H}_k + [\mathcal{H}_k]^T}{2}, \quad (5c)$$

where, in execution order, Eq. (5c) ensures that the Hessian approximation is symmetric as the analytical Hessian, then Eq. (5b) with $0 < \varepsilon \ll 1$ guarantees positive-definiteness, and finally Eq. (5a) stabilizes the estimator by introducing inertia from previous iterations, starting from an identity at the zeroth iteration, $\bar{\mathcal{H}}_0 = I$.

The simultaneous perturbation stochastic approximation to the Hessian matrix \mathcal{H}_k is given by [98]

$$\mathcal{H}_k(\boldsymbol{\theta}) = \frac{\mathbf{g}_k(\boldsymbol{\theta} + \tilde{b}_k \tilde{\Delta}_k) - \mathbf{g}_k(\boldsymbol{\theta})}{\tilde{b}_k} \begin{pmatrix} 1/\tilde{\Delta}_{k,1} \\ \vdots \\ 1/\tilde{\Delta}_{k,p} \end{pmatrix}^T, \quad (6)$$

which can be rewritten by components as

$$[\mathcal{H}_k]_{ij} = \frac{\delta^2 f_k(\boldsymbol{\theta})}{2b_k \tilde{b}_k \Delta_{k,i} \tilde{\Delta}_{k,j}}, \quad (7)$$

where

$$\begin{aligned} \delta^2 f_k(\boldsymbol{\theta}) &= f(\boldsymbol{\theta} + b_k \Delta_k + \tilde{b}_k \tilde{\Delta}_k) - f(\boldsymbol{\theta} + b_k \Delta_k) \\ &\quad - f(\boldsymbol{\theta} - b_k \Delta_k + \tilde{b}_k \tilde{\Delta}_k) + f(\boldsymbol{\theta} - b_k \Delta_k), \end{aligned} \quad (8)$$

$\tilde{b}_k = \tilde{b}/k^t$ is a gain series similar in nature to b_k , and $\tilde{\Delta}_k$ is a random vector formed by p components uniformly generated from the set $\{\pm 1\}$ analogous to Δ_k . Thereby, 2SPSA requires a total of 4 objective function evaluations at each iteration.

An iteration of this method is given by Eqs. (8), (6), (5), (4), and (2).

3. QN-SPSA

The rationale behind the gradient descent method is to reach a local minimum by moving, at each iteration, along the direction of steepest descent of the objective function in the parameter space, $-(\partial f / \partial \boldsymbol{\theta})^T$, while limiting the magnitude of the

update step, $\Delta\boldsymbol{\theta}$. The steepest descent rule can be obtained by choosing the increment as

$$\Delta\boldsymbol{\theta} = \arg \min_{\Delta\boldsymbol{\theta} \in \mathbb{R}^{2p}} \left\{ \left\langle \left(\frac{\partial f}{\partial \boldsymbol{\theta}} \right)^T, \Delta\boldsymbol{\theta} \right\rangle + \frac{1}{2\eta} \|\Delta\boldsymbol{\theta}\|_2^2 \right\}, \quad (9)$$

where $\eta \in \mathbb{R}^+$ is the learning rate, $\langle \boldsymbol{\theta}, \boldsymbol{\theta}' \rangle = \boldsymbol{\theta}^T \boldsymbol{\theta}'$ is the inner product for two vectors $\boldsymbol{\theta}$ and $\boldsymbol{\theta}'$, respectively, and $\|\cdot\|_2 = \sqrt{\langle \cdot, \cdot \rangle}$ is the l^2 norm. Differentiating the argument on the right hand side of Eq. (9) with respect to $\Delta\boldsymbol{\theta}$ and setting it to 0, provides the well-known gradient descent step

$$\Delta\boldsymbol{\theta} = -\eta \left(\frac{\partial f}{\partial \boldsymbol{\theta}} \right)^T. \quad (10)$$

This result relies on l^2 geometry, where a displacement on any direction in the parameter space is treated equally. However, it is reasonable to consider that the objective function may not be equally sensible to changes on different parameters, and therefore, that a fitter notion of distance would measure the length of the step $\Delta\boldsymbol{\theta}$ by weighting changes on each parameter differently. This is addressed by a method called natural gradient descent [99], which endows the parameter space with a suitable metric \mathcal{G} and induces the norm $\|\cdot\|_{\mathcal{G}} = \sqrt{\langle \cdot, \mathcal{G} \cdot \rangle}$. Then, the increment is stated as

$$\Delta\boldsymbol{\theta} = \arg \min_{\Delta\boldsymbol{\theta} \in \mathbb{R}^{2p}} \left\{ \left\langle \left(\frac{\partial f}{\partial \boldsymbol{\theta}} \right)^T, \Delta\boldsymbol{\theta} \right\rangle + \frac{1}{2\eta} \|\Delta\boldsymbol{\theta}\|_{\mathcal{G}}^2 \right\}, \quad (11)$$

which leads to the natural gradient descent rule

$$\boldsymbol{\theta}_{k+1} = \boldsymbol{\theta}_k - \eta [\mathcal{G}(\boldsymbol{\theta}_k)]^{-1} \left(\frac{\partial f}{\partial \boldsymbol{\theta}}(\boldsymbol{\theta}_k) \right)^T. \quad (12)$$

The quantum natural method, which takes \mathcal{G} to be the Fubini-Study metric tensor, results particularly useful to improve the convergence rates for optimization problems in quantum applications [75]. The Fubini-Study metric tensor is proportional to the Quantum Fisher Information matrix, so its computation may result very expensive when many variables are involved. To tackle this problem Gacon *et al.* [78] took advantage of the similarity between the Eqs. (12) and (3), along with the possibility of writing the Fubini-Study metric tensor as

$$\mathcal{G}(\boldsymbol{\theta}) = -\frac{1}{2} \left[\frac{\partial}{\partial \boldsymbol{\theta}} \left(\frac{\partial F(\boldsymbol{\theta}', \boldsymbol{\theta})}{\partial \boldsymbol{\theta}} \right)^T \right] \bigg|_{\boldsymbol{\theta}'=\boldsymbol{\theta}}, \quad (13)$$

where $F(\boldsymbol{\theta}', \boldsymbol{\theta})$ is the fidelity between two quantum states parameterized with the variables $\boldsymbol{\theta}'$ and $\boldsymbol{\theta}$, respectively. In particular, the discretization scheme from the 2SPSA algorithm is reused and the original Hessian approximation is adapted from acting on the objective function to acting on the Fubini-Study metric by perturbing only one of its arguments. In this manner, Gacon *et al.* proposed a stochastic approximation based on the quantum natural method, called quantum natural SPSA (QN-SPSA), which avoids the curse of dimensionality. In order to reuse the equations already presented for

the 2SPSA method, we will abuse notation and denote \mathcal{H} the Hessian estimate of the Fubini-Study metric, yielding

$$[\mathcal{H}_k]_{ij} = -\frac{\delta^2 F_k(\boldsymbol{\theta}_k)}{4b_k \tilde{b}_k \Delta_{k,i} \tilde{\Delta}_{k,j}}, \quad (14)$$

where

$$\begin{aligned} \delta^2 F_k(\boldsymbol{\theta}) &= F(\boldsymbol{\theta}, \boldsymbol{\theta} + b_k \Delta_k + \tilde{b}_k \tilde{\Delta}_k) \\ &\quad - F(\boldsymbol{\theta}, \boldsymbol{\theta} + b_k \Delta_k) \\ &\quad - F(\boldsymbol{\theta}, \boldsymbol{\theta} - b_k \Delta_k + \tilde{b}_k \tilde{\Delta}_k) \\ &\quad + F(\boldsymbol{\theta}, \boldsymbol{\theta} - b_k \Delta_k), \end{aligned} \quad (15)$$

and Δ and $\tilde{\Delta}$ are two vectors of p components randomly sampled from the set $\{\pm 1\}$.

Furthermore, following the same logic as in the 2SPSA algorithm, the simultaneous perturbation stochastic approximation of the Hessian Eq. (14) must be conditioned by following the procedure on the system of Eqs. (5). Note that while we are re-using the discretization scheme and update rule from 2SPSA, this is a first-order method, as the conditioner \mathcal{H}_k comes not from a second-order expansion on the target function, but only from a re-interpretation of the notion of distance in the parameter space. Nevertheless, requiring only two measurements of the objective function makes this algorithm specially suitable for problems where the metric tensor can be efficiently computed; that is, cases where the evaluation of the fidelity F between two known pure quantum states requires marginal resources in contrast to the potentially expensive target function f .

Finally, an iteration of this method is given by Eqs. (15), (14), (5), (4), and (2).

B. Complex-variable methods

Our goal is now to solve the optimization problem for a real function on complex variables, which we will emphasize by denoting the complex argument as \mathbf{z} . Then, let f be a real function on complex variables $f : \mathbf{z} \in \mathbb{C}^p \rightarrow \mathbb{R}$. It is clear that any nontrivial function f cannot accomplish the Cauchy-Riemann conditions, or equivalently, that f also depends upon $\mathbf{z}^* \in \mathbb{C}^p$, where \mathbf{z}^* denotes the complex conjugate of \mathbf{z} . To study non-holomorphic functions we use the Wirtinger calculus [86] by considering the paired shorthand variable $\boldsymbol{\mu} = (\mathbf{z}, \mathbf{z}^*)^T \in \mathbb{C}^{2p}$ rather than only \mathbf{z} . However, in practice we solve the corresponding results only for \mathbf{z} instead of $\boldsymbol{\mu}$.

Bearing the complete dependence upon $\boldsymbol{\mu}$ and considering a complex increment $\Delta\boldsymbol{\mu} = (\Delta\mathbf{z}, \Delta\mathbf{z}^*)^T$, one can expand

$$f(\boldsymbol{\mu} + \Delta\boldsymbol{\mu}) = f(\boldsymbol{\mu}) + \frac{\partial f}{\partial \boldsymbol{\mu}} \Delta\boldsymbol{\mu} + \frac{1}{2} \Delta\boldsymbol{\mu}^\dagger \mathcal{H} \Delta\boldsymbol{\mu} + \dots, \quad (16)$$

where

$$\mathcal{H} = \frac{\partial}{\partial \boldsymbol{\mu}} \left(\frac{\partial f}{\partial \boldsymbol{\mu}} \right)^\dagger \quad (17)$$

is the complex Hessian of the function f [87], the symbol (\dagger) denotes the conjugate transpose, and differentiation with respect to $\boldsymbol{\mu}$ is defined by

$$\frac{\partial f}{\partial \boldsymbol{\mu}} = \begin{pmatrix} \frac{\partial f}{\partial \mathbf{z}} & \frac{\partial f}{\partial \mathbf{z}^*} \end{pmatrix}. \quad (18)$$

Also note that the inner product of any two vectors written in this paired complex-conjugate representation is real since, for arbitrary $\boldsymbol{\mu} = (\mathbf{z}, \mathbf{z}^*)^T$ and $\boldsymbol{\mu}' = (\mathbf{z}', \mathbf{z}'^*)^T$, with $\mathbf{z}, \mathbf{z}' \in \mathbb{C}^p$, yields

$$\boldsymbol{\mu}^\dagger \boldsymbol{\mu}' = (\mathbf{z}^* \quad \mathbf{z}) \begin{pmatrix} \mathbf{z}' \\ \mathbf{z}'^* \end{pmatrix} = 2 \operatorname{Re}\{\mathbf{z}^\dagger \mathbf{z}'\}. \quad (19)$$

1. CSPSA

Taking a first-order approximation on $|\Delta\boldsymbol{\mu}|$ from Eq. (16), the largest decrease of the function f given by

$$f(\boldsymbol{\mu} + \Delta\boldsymbol{\mu}) - f(\boldsymbol{\mu}) \approx \frac{\partial f}{\partial \boldsymbol{\mu}} \Delta\boldsymbol{\mu}, \quad (20)$$

is accomplished for a perturbation $\Delta\boldsymbol{\mu}$ in the direction of $-(\partial f / \partial \boldsymbol{\mu})^\dagger$, providing the complex equivalent to the gradient descent update rule,

$$\boldsymbol{\mu}_{k+1} = \boldsymbol{\mu}_k - \eta \left(\frac{\partial f}{\partial \boldsymbol{\mu}} \right)^\dagger, \quad (21)$$

where $\eta \in \mathbb{R}^+$ is the learning rate.

Taking the first row of Eq. (21) yields a stochastic approximation which Utreras-Alarcón *et al.* [19] use to introduce the CSPSA algorithm given by the iterative rule

$$\mathbf{z}_{k+1} = \mathbf{z}_k - a_k \mathbf{g}_k(\mathbf{z}_k), \quad (22)$$

where $a_k = a / (k + A)^s$. The gradient estimator is now given by

$$\mathbf{g}_k(\mathbf{z}) = \frac{f(\mathbf{z} + b_k \Delta_k) - f(\mathbf{z} - b_k \Delta_k)}{2b_k} \begin{pmatrix} 1/\Delta_{k,1}^* \\ \vdots \\ 1/\Delta_{k,p}^* \end{pmatrix}, \quad (23)$$

with $b_k = b/k^t$, and Δ_k is a random vector with p components uniformly generated from the set $\{\pm 1, \pm i\}$, with i the imaginary unit, to span any possible direction in the complex space. Note that to avoid the excessive cluttering of the notation, we have omitted the dependence of \mathbf{g}_k on \mathbf{z}^* . In the following we write $\mathbf{g}_k(\mathbf{z}, \mathbf{z}^*)$ as $\mathbf{g}_k(\mathbf{z})$, likewise for other functions.

An iteration of the CSPSA algorithm is given by Eqs. (23) and (22).

2. 2CSPSA

To obtain a second-order iteration rule, we take up to second-order terms on $|\Delta\boldsymbol{\mu}|$ from expansion (16) and consider the problem of finding the optimal perturbation $\Delta\boldsymbol{\mu}$ that

makes $f(\boldsymbol{\mu} + \Delta\boldsymbol{\mu})$ a minimum value of f . Such a step is found by taking $\partial f(\boldsymbol{\mu} + \Delta\boldsymbol{\mu})/\partial\Delta\boldsymbol{\mu} = 0$, which reduces to

$$\left[\frac{\partial}{\partial\boldsymbol{\mu}} \left(\frac{\partial f}{\partial\boldsymbol{\mu}} \right)^\dagger \right] \Delta\boldsymbol{\mu} = - \left(\frac{\partial f}{\partial\boldsymbol{\mu}} \right)^\dagger, \quad (24)$$

and can be rewritten in terms of \mathbf{z} and \mathbf{z}^* as

$$\begin{pmatrix} \mathcal{H}_{zz} & \mathcal{H}_{zz^*} \\ \mathcal{H}_{z^*z} & \mathcal{H}_{z^*z^*} \end{pmatrix} \begin{pmatrix} \Delta\mathbf{z} \\ \Delta\mathbf{z}^* \end{pmatrix} = - \begin{pmatrix} [\partial f/\partial\mathbf{z}]^\dagger \\ [\partial f/\partial\mathbf{z}^*]^\dagger \end{pmatrix}, \quad (25)$$

where the elements of the block matrix are

$$\mathcal{H}_{zz} = \frac{\partial}{\partial\mathbf{z}} \left(\frac{\partial f}{\partial\mathbf{z}} \right)^\dagger, \quad (26)$$

$$\mathcal{H}_{zz^*} = \frac{\partial}{\partial\mathbf{z}} \left(\frac{\partial f}{\partial\mathbf{z}^*} \right)^\dagger, \quad (27)$$

$$\mathcal{H}_{z^*z} = \mathcal{H}_{zz^*}^\dagger, \text{ and} \quad (28)$$

$$\mathcal{H}_{z^*z^*} = \mathcal{H}_{zz}^*. \quad (29)$$

The system of Eqs. (25) can be solved for $\Delta\mathbf{z}$ as

$$\begin{aligned} \Delta\mathbf{z} &= (\mathcal{H}_{zz} - \mathcal{H}_{z^*z} \mathcal{H}_{z^*z^*}^{-1} \mathcal{H}_{zz^*})^{-1} \\ &\quad \times \left\{ \mathcal{H}_{z^*z} \mathcal{H}_{z^*z^*}^{-1} \left(\frac{\partial f}{\partial\mathbf{z}^*} \right)^\dagger - \left(\frac{\partial f}{\partial\mathbf{z}} \right)^\dagger \right\}, \end{aligned} \quad (30)$$

which is the update step corresponding to a Newton algorithm [87]. While this solution requires a large number of operations, it may be greatly simplified by taking a block-diagonal approximation, $\mathcal{H}_{zz^*} \approx 0$, yielding a pseudo-Newton method [100] with

$$\Delta\mathbf{z} = -\mathcal{H}_{zz}^{-1} \left(\frac{\partial f}{\partial\mathbf{z}} \right)^\dagger, \quad (31)$$

which also has the advantage of being operationally independent of \mathbf{z}^* in practice.

Analog to the 2SPSA algorithm, in the stochastic approximation, we take the descent direction given by (31). Thereby, we define the 2CSPSA algorithm by the update rule

$$\mathbf{z}_{k+1} = \mathbf{z}_k - \bar{a}_k [\bar{\mathcal{H}}_k(\mathbf{z}_k)]^{-1} \mathbf{g}_k(\mathbf{z}_k), \quad (32)$$

where $\bar{a}_k = 1/(k+A)^s$, $\mathbf{g}_k(\mathbf{z})$ is given by Eq. (23), and $\bar{\mathcal{H}}_k$ is a modified version of the simultaneous perturbation stochastic approximation for the partial complex Hessian, \mathcal{H}_{zz} at the k -th iteration. Similar to the system of Eqs. (5) for the real-variable case, $\bar{\mathcal{H}}_k$ is computed through the sequence

$$\bar{\mathcal{H}}_k = \frac{k}{k+1} \bar{\mathcal{H}}_{k-1} + \frac{1}{k+1} \mathcal{H}_k'' \quad (33a)$$

$$\mathcal{H}_k'' = \sqrt{\mathcal{H}_k'^2 + \varepsilon I} \quad (33b)$$

$$\mathcal{H}_k' = \frac{\mathcal{H}_k + [\mathcal{H}_k]^\dagger}{2}, \quad (33c)$$

where, in execution order, Eq. (33c) makes the Hessian approximation hermitian as the exact Hessian, Eq. (33b) with

$0 < \varepsilon \ll 1$ ensures positive-definiteness, and finally Eq. (33a) stabilizes the estimator by introducing inertia from previous iterations, starting from an identity at the zeroth iteration, $\bar{\mathcal{H}}_0 = I$. Note that the regularization (33b) is still valid in the complex-variable case since its input, \mathcal{H}_k' , has real eigenvalues due to the previous hermitization (33c).

In this case, following the simultaneous perturbation stochastic approximation approach for the partial complex Hessian \mathcal{H}_{zz} yields by components

$$[\mathcal{H}_k(\mathbf{z})]_{ij} = \frac{\delta^2 f_k(\mathbf{z})}{2b_k \tilde{b}_k \Delta_{k,i} \tilde{\Delta}_{k,j}^*}, \quad (34)$$

where

$$\begin{aligned} \delta^2 f_k(\mathbf{z}) &= f(\mathbf{z} + b_k \Delta_k + \tilde{b}_k \tilde{\Delta}_k) - f(\mathbf{z} + b_k \Delta_k) \\ &\quad - f(\mathbf{z} - b_k \Delta_k + \tilde{b}_k \tilde{\Delta}_k) + f(\mathbf{z} - b_k \Delta_k), \end{aligned} \quad (35)$$

and Δ and $\tilde{\Delta}$ are two random vectors, each composed by p elements uniformly generated from the set $\{\pm 1, \pm i\}$.

Note that this method requires the inversion and regularization of a $p \times p$ hermitian complex matrix, while the analog 2SPSA optimization of an equivalent problem would require the inversion and regularization of a $2p \times 2p$ symmetric real matrix.

An iteration of this method is given by Eqs. (35), (34), (33), (32), and (23).

3. QN-CSPSA

In the work of Yao *et al.* [88], the natural gradient method was adapted for a complex parameter space by posing the usual natural gradient update rule (12) with the relevant metric \mathcal{G} and using an invertible linear transformation W to move back and forth between the real and complex parametrizations such that

$$W \begin{pmatrix} \mathbf{x} \\ \mathbf{y} \end{pmatrix} = \begin{pmatrix} \mathbf{x} + i\mathbf{y} \\ \mathbf{x} - i\mathbf{y} \end{pmatrix} := \begin{pmatrix} \mathbf{z} \\ \mathbf{z}^* \end{pmatrix}, \quad (36)$$

where $\mathbf{x}, \mathbf{y} \in \mathbb{R}^p$. However, continuously moving between parametrizations is undesirable, and therefore here we present a natively complex implementation of the natural gradient method for quantum applications, which is developed in an analogous way to the QN-SPSA method.

The complex gradient descent rule (21) can be obtained as a solution of the optimization problem

$$\Delta\boldsymbol{\mu} = \arg \min_{\Delta\boldsymbol{\mu} \in \mathbb{C}^{2p}} \left\{ \left\langle \left(\frac{\partial f}{\partial\boldsymbol{\mu}} \right)^\dagger, \Delta\boldsymbol{\mu} \right\rangle + \frac{1}{2\eta} \|\Delta\boldsymbol{\mu}\|_2^2 \right\}, \quad (37)$$

where $\eta \in \mathbb{R}^+$ is the learning rate, $\langle \boldsymbol{\mu}, \boldsymbol{\mu}' \rangle = \boldsymbol{\mu}^\dagger \boldsymbol{\mu}'$ is the inner product for two complex vectors $\boldsymbol{\mu}$ and $\boldsymbol{\mu}'$, respectively, and $\|\cdot\|_2 = \sqrt{\langle \cdot, \cdot \rangle}$ is the l^2 norm.

As in the real case, to require the parameter update to remain small in the space endowed with metric \mathcal{G} , the l^2 norm

is replaced in Eq. (37) by $\|\cdot\|_{\mathcal{G}} = \sqrt{\langle \cdot, \mathcal{G} \cdot \rangle}$ to obtain

$$\Delta\boldsymbol{\mu} = \arg \min_{\Delta\boldsymbol{\mu} \in \mathbb{C}^{2p}} \left\{ \left\langle \left(\frac{\partial f}{\partial \boldsymbol{\mu}} \right)^{\dagger}, \Delta\boldsymbol{\mu} \right\rangle + \frac{1}{2\eta} \|\Delta\boldsymbol{\mu}\|_{\mathcal{G}}^2 \right\}, \quad (38)$$

which leads to

$$\Delta\boldsymbol{\mu} = -\eta \mathcal{G}^{-1} \left(\frac{\partial f}{\partial \boldsymbol{\mu}} \right)^{\dagger}, \quad (39)$$

where \mathcal{G} is an hermitian matrix.

In the case of pure quantum states, we choose the metric \mathcal{G} given by a quarter of the complex Quantum Fisher Information matrix [101], that is,

$$\mathcal{G} = -\frac{1}{2} \left[\frac{\partial}{\partial \boldsymbol{\mu}} \left(\frac{\partial F(\boldsymbol{\mu}', \boldsymbol{\mu})}{\partial \boldsymbol{\mu}} \right)^{\dagger} \right] \Big|_{\boldsymbol{\mu}'=\boldsymbol{\mu}}, \quad (40)$$

where $F(\boldsymbol{\mu}', \boldsymbol{\mu})$ is the fidelity between two states parameterized with variables $\boldsymbol{\mu}'$ and $\boldsymbol{\mu}$, respectively.

Taking, as in the 2CSPSA case a block-diagonal approximation of \mathcal{G} , the first row of Eq. (39) yields

$$\Delta\boldsymbol{z} = -\eta \mathcal{G}_{zz}^{-1} \left(\frac{\partial f}{\partial \boldsymbol{z}} \right)^{\dagger}, \quad (41)$$

where \mathcal{G}_{zz} is the top left block of \mathcal{G} .

Given the Hessian form of \mathcal{G}_{zz} and considering the similarity of Eqs. (41) and (31), we can borrow the discretization scheme from 2CSPSA to approximate \mathcal{G}_{zz} . Abusing notation and denoting \mathcal{H}_k the simultaneous perturbation stochastic approximation of \mathcal{G}_{zz} at iteration k , allows to reuse the equations already presented for 2CSPSA yielding

$$[\mathcal{H}_k]_{ij} = -\frac{\delta^2 F_k(\boldsymbol{z}_k)}{4b_k \tilde{b}_k \Delta_{k,i} \tilde{\Delta}_{k,j}^*}, \quad (42)$$

with

$$\begin{aligned} \delta^2 F_k(\boldsymbol{z}) &= F(\boldsymbol{z}, \boldsymbol{z} + b_k \boldsymbol{\Delta}_k + \tilde{b}_k \tilde{\boldsymbol{\Delta}}_k) \\ &\quad - F(\boldsymbol{z}, \boldsymbol{z} + b_k \boldsymbol{\Delta}_k) \\ &\quad - F(\boldsymbol{z}, \boldsymbol{z} - b_k \boldsymbol{\Delta}_k + \tilde{b}_k \tilde{\boldsymbol{\Delta}}_k) \\ &\quad + F(\boldsymbol{z}, \boldsymbol{z} - b_k \boldsymbol{\Delta}_k), \end{aligned} \quad (43)$$

and conditioning as in the system of Eqs. (33). As before, $\boldsymbol{\Delta}$ and $\tilde{\boldsymbol{\Delta}}$ are two random vectors, each composed by p elements uniformly generated from the set $\{\pm 1, \pm i\}$.

Finally, an iteration of this method which we call quantum natural CSPSA (QN-CSPSA) is given by Eqs. (43), (42), (33), (32), and (23).

III. APPLICATIONS

The performance of the introduced methods is studied comparing their rate of convergence and focusing on the number of evaluations (or measurements) of the objective function or

quantum circuits as main resources. We study the convergence of the optimization methods in three important applications: variational quantum eigensolver, quantum control, and quantum state estimation. We use a variational quantum eigensolver to obtain the ground state energy of the Heisenberg Hamiltonian, which is an ubiquitous and relatively simple model that describes the interactions within a chain of spins. We implement the GRAdient Ascent Pulse Engineering (GRAPE) method [94], which is used to engineer quantum states. This method approximates a control pulse by a sequence of constant intensity pulses. The control parameters of this pulse are optimized in order to find the best implementation of a given state, even in the presence of noise [9]. Finally, in quantum state estimation we implement Self-Guided Quantum Tomography (SGQT) [17], which is based on the minimization of the infidelity between an unknown state and a known parametrized state. Since the studied optimization methods are stochastic in nature we use numerical simulations and estimate mean, variance (or standard deviation), median, and interquartile range. Measurements are simulated using a finite sample of various sizes. The simulations consider two set of gain parameters: standard with $a = 3$, $b = 0.1$, $A = 0$, $s = 0.602$, and $t = 0.101$, and asymptotic with $a = 3$, $b = 0.1$, $A = 0$, $s = 1$, and $t = 0.166$. For both sets, we take $\tilde{b} = 0.1$ as well. As for the regularization procedures, we set the value $\varepsilon = 10^{-3}$, which provides good results in our numerical experiments.

A. Variational Quantum Eigensolver

Searching for the ground state and its energy E_0 of a given Hamiltonian is a problem of great interest in areas such as computational chemistry and condensed matter physics. This is due to the fact that much of the phenomenology and properties of quantum systems can be studied from the ground state and its energy. However, finding this eigenstate on large systems is not a trivial task, and more than often directly infeasible due to the exponential growth of the Hilbert space dimension with respect to the number of subsystems. For large systems, the Rayleigh-Ritz method [102, 103] is a useful tool as it restricts itself to search on a parametrised subset of the original Hilbert space to reduce the computational cost of the optimization. A further reduction in the computational cost is achieved using the variational quantum eigensolver [104] (VQE) method, which consists of performing the Rayleigh-Ritz method for a given Hamiltonian with the help of a quantum and a classical computer, making it a promising tool for the current generation of quantum technologies.

To formalize the problem, the goal is to find the eigenstates $|\psi\rangle$ associated with the lower eigenvalue E_0 of a Hamiltonian. This ground state can be characterized as the solution to the optimization problem

$$E_0 = \min_{|\psi\rangle} \frac{\langle \psi | H | \psi \rangle}{\langle \psi | \psi \rangle}. \quad (44)$$

The Rayleigh-Ritz method provides an estimate for E_0 by parametrizing the trial states as $|\psi(\theta)\rangle$ and carrying the opti-

mization over the vector θ of parameters. The underlying idea is that the subset defined by the parametrization must have a lower dimension than the total Hilbert space in order to reduce the computation cost.

The VQE method considers the generic hermitian Hamiltonian operator $H = \sum_{i=1}^n h_i \sigma_i$ and the trial state parametrization

$$|\psi(\theta)\rangle = R_N(\theta_N) \cdots R_1(\theta_1)|0\rangle, \quad (45)$$

where $R_i(\theta_i)$ are quantum gates parametrized by θ_i and applied one after another to the initial state $|0\rangle$. This parametrization corresponds to a variational quantum circuit. The average energy $\langle\psi(\theta)|H|\psi(\theta)\rangle$ can then be computed by individually measuring each term $\langle\psi(\theta)|\sigma_i|\psi(\theta)\rangle$ on a quantum computer and adding the results weighted with their respective coefficients h_i . Thereafter, the values of $\langle\psi(\theta)|H|\psi(\theta)\rangle$ are used to feed a suitable optimization method that is executed on a classical computer. As long as the individual terms $\langle\psi(\theta)|\sigma_i|\psi(\theta)\rangle$ can be measured more efficiently than evaluating on a classical computer, the VQE method leads to a computational advantage.

Typically, the VQE method employs SPSA as the optimization algorithm due to its robustness against noise, which suggests that the other optimization methods presented here can also be used. In order to evaluate the performance of these various methods, we turned as a testing ground to the problem of finding the ground state energy of the Heisenberg Hamiltonian, which models the magnetic interaction of a ferromagnetic lattice. This is given by the expression

$$H = j \sum_{\langle m, n \rangle} (X_m X_n + Y_m Y_n + Z_m Z_n) + h \sum_m Z_m, \quad (46)$$

where j is the coupling constant, h the interaction with an external magnetic field, and X, Y, Z are single-qubit Pauli operators. To parametrize the trial state we use the complex parametric single-qubit gate

$$W(z) = e^{-i(z\sigma_+ + z^*\sigma_-)}, \quad (47)$$

where z is a complex parameter and $\sigma_{\pm} = X \pm Y$. This gate can be experimentally implemented by a sequence of three real parameter gates.

The parametrization used for the trial state is given by

$$|\psi(z)\rangle = \prod_{q=1}^N W_q^d(z_q^d) U_{\text{ENT}} \times \cdots \times \prod_{q=1}^N W_q^1(z_q^1) U_{\text{ENT}} \prod_{q=1}^N W_q^0(z_q^0) |0\rangle, \quad (48)$$

where W_q^l corresponds to applying W on the q^{th} qubit, l symbolizes the layer of the circuit, and U_{ENT} is a three-qubit entangling gate depicted in Fig. 1. Similarly for z_q^l .

To evaluate the performance of the different algorithms we consider the Heisenberg Hamiltonian Eq. (46) for a triangular lattice of 3 qubits with $h = j = 1$. The trial states are

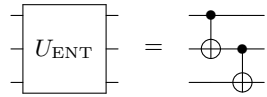


FIG. 1: Entangling gate U_{ENT} .

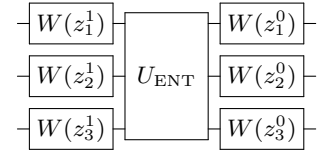


FIG. 2: Parametric circuit used in the implementation of VQE for the Heisenberg Hamiltonian of three qubits. U_{ENT} is an entangling gate depicted in Fig. 1.

parametrized by Eq. (48) with $d = 1$ layers, which is depicted by the circuit in Fig. 2.

The results of the numerical simulations are depicted in Fig. 3. For each algorithm the optimization process is repeated using 10^4 initial vectors of parameters, which are randomly generated according to the uniform Haar distribution, and 10^3 iterations. As a function of the number of circuits employed, we calculate the mean and standard deviation (upper row, solid line and shaded area, respectively) and median and interquartile range (lower row, solid line and shaded area, respectively) of the sample of ground energy estimates. From left to right, the columns show SPSA (blue solid line) and CSPSA (red solid line), 2SPSA (blue solid line) and 2CSPSA (red solid line), NG-SPSA (blue solid line) and NG-CSPSA (red solid line). The black dashed line indicates the exact value of the ground state energy $E_0 = -6$. The gain coefficients used were the standard gains for second-order methods and the asymptotic gains for the remaining methods, as this choice yielded better results. The circuits and measurements were simulated using the Yao package framework [105].

As Fig. 3 clearly shows, neither SPSA nor CSPSA achieved mean convergence toward the ground energy. In the case of CSPSA, however, median convergence is achieved after 15000 circuit evaluations while SPSA is still far from the ground energy value. This indicates that optimization through CSPSA and SPSA leads to some realizations that are characterized by ground state energy estimates that are far from the true value. The number of this class of realizations is, in the case of SPSA, high enough to prevent convergence from being achieved.

Second-order methods exhibit a very different behavior. Both 2CSPSA and 2SPSA achieve mean convergence, with 2SPSA being marginally faster than 2CSPSA, after 15000 circuit evaluations and with similar standard deviations. In median, however, both methods reach convergence much faster than the first-order methods, that is, after just 5000 circuit evaluations. Moreover, both methods exhibit an almost identical behavior and very narrow interquartile ranges. The difference between the mean and median convergence indicates the

presence of realizations that converge at a lower rate. Let us note that the interquartile ranges of the second-order methods lay below the interquartile range of the first-order methods, which occurs approximately up to 15000 circuits. Thereby, almost 75% of the best realization of the second-order methods show better ground energy estimates than the 75% of the worst ground energy estimates provided by the first-order methods.

The QN-SPSA and QN-CSPSA algorithms show a behavior with characteristics similar to those of the first and second-order methods. On the one hand, QN-SPSA and QN-CSPSA do not reach the mean convergence and have a very wide standard deviation, both of which are very similar to the first-order methods. On the other hand, median convergence resembles almost exactly the case of the second-order methods. In this case, however, the interquartile range is much wider than the generated by the second-order methods. Thus, QN-SPSA and QN-CSPSA present a much higher number of slow-convergence realizations than second-order methods. QN-SPSA and QN-CSPSA also show an advantage with respect to CSPSA and SPSA. In contrast to these algorithms, after 1000 circuits, QN-SPSA and QN-CSPSA reached median convergence and comparatively narrower interquartile ranges.

Thus, the 2CSPSA and 2SPSA algorithms provide an advantage over CSPSA, SPSA, QN-CSPSA and QN-SPSA algorithms. Moreover, after 10000 circuits (or 209 iterations) approximately 75% of the realizations by the second-order methods has already achieve a value very close to the true ground-state energy.

B. Quantum Control

Quantum control theory allows to establish a firm theoretical basis and to develop a series of systematic methods for the active manipulation and control of quantum systems, in particular the search for an optimized time evolution that allows to guide the system from an initial state to a desired final state. Quantum control theory has already attained significant successes in physical chemistry [106], atomic and molecular physics [107] and quantum optics [108] and has also contributed to the understanding of fundamental aspects of quantum mechanics [109]. In recent years, the development of the general principles of quantum control theory has been recognized as an essential requirement for the future application of quantum technologies.

A particular problem in quantum control is the accurate engineering of quantum states, that is, whether one can drive a quantum system to a desired state. This problem has practical importance since it has a close connection with the universality of quantum computation and the possibility of achieving atomic or molecular scale transformations. A common research approach is that of quantum systems of finite dimension (finite level) for which the controllability criteria can be expressed in terms of parameters included in the Hamiltonian of the system.

The quantum state control problem [110] is to identify an appropriate set of control parameters $u_k(t) \in \mathbb{C}$, which are

coupled to the system through the interaction Hamiltonian

$$H(t) = H_0 + \sum_k \left(u_k(t) H_k + u_k^*(t) H_k^\dagger \right), \quad (49)$$

in such a way that they guide the evolution of the system from an initial state $|\psi_0\rangle$ to a predetermined target state $|\psi_f\rangle$. In order to obtain this set of parameters, it is necessary to solve the Schrödinger equation. However, the solutions of the Schrödinger equation for a time-dependent Hamiltonian are generally not possible to obtain analytically. It is possible in certain cases to resort to techniques developed in the area of adiabatic control [111–114].

To overcome this problem we use the GRadient Ascent Pulse Engineering (GRAPE) method [94], originally introduced in nuclear magnetic resonance spectroscopy and proposed to design a pulse sequence that drives the evolution toward the optimum of a predefined objective function. This method allows us to calculate the evolution of a time-dependent Hamiltonian through a sequence of time-independent Hamiltonians H_m . The total evolution time T is divided into a number M of time intervals Δt_m (usually of equal length) so that in each interval the control parameters $u_k(t)$ are constant. On each time interval the evolution is given by

$$U_m = e^{-i\Delta t_m H_m}, \quad (50)$$

where $H_m = H(t_m)$. A classical optimization algorithm is used to obtain the values of the control parameters that lead to the optimal of the objective function.

The evolution of the system at time T is thus

$$U_{\text{GRAPE}} = \prod_{m=0}^{M-1} U_m \quad (51)$$

and the state of the system at time T is

$$|\tilde{\psi}_f\rangle = U_{\text{GRAPE}} |\psi_0\rangle. \quad (52)$$

Once a propagator has been computed for a set of control parameters, all that remains is to choose a function to compare the target state with the state given by an evolution for a certain set of control parameter values. In our case we use the infidelity that is given by

$$I(|\tilde{\psi}_f\rangle, |\psi_f\rangle) = 1 - |\langle \tilde{\psi}_f | \psi_f \rangle|^2. \quad (53)$$

This objective function is minimized with an optimization algorithm. The original GRAPE proposal uses the descending gradient algorithm.

To test the optimization methods here introduced, we resort to quantum control of a one- and two-qubit system. In the single-qubit case we chose as target state the ground state $|\psi_f\rangle = |0\rangle$ of the Hamiltonian

$$H(t) = \frac{1}{2} \sigma_z + \frac{1}{2} (u(t) \sigma_+ + u^*(t) \sigma_-), \quad (54)$$

which depends on a single complex control parameter $u(t)$. This scenario describes for instance the evolution of 1/2-spin particle interacting with a classical electromagnetic field.

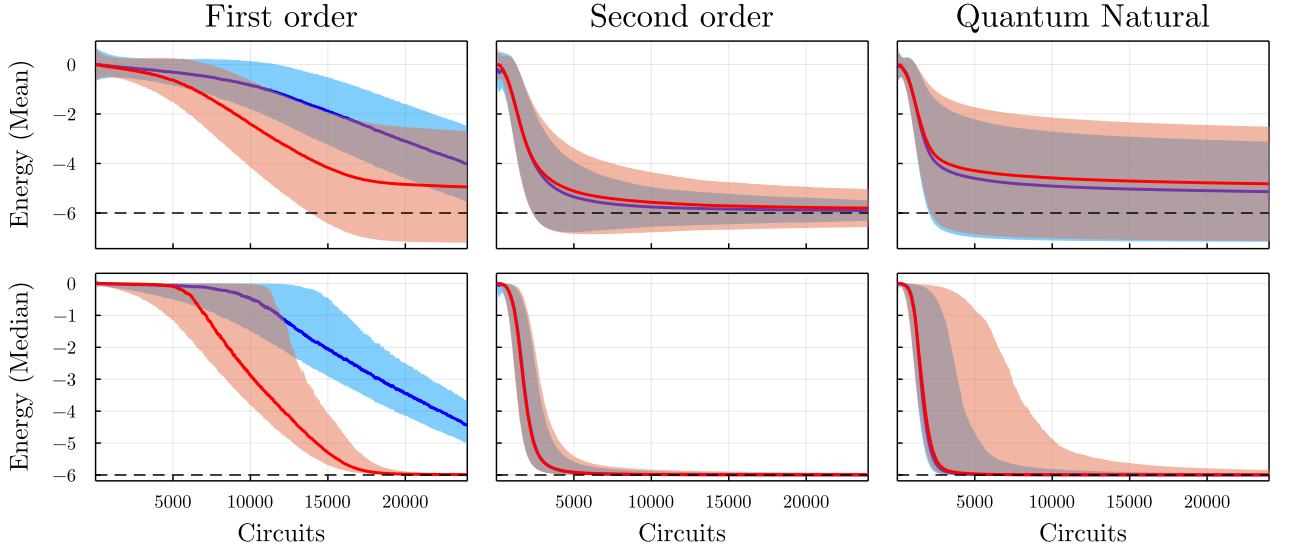


FIG. 3: The mean (top) and median (bottom) of the ground state energy estimate as a function of the number of circuits obtained by performing VQE on the Heisenberg Hamiltonian. From left to right, the columns show SPSA (blue solid line) and CSPSA (red solid line), 2SPSA (blue solid line) and 2CSPSA (red solid line), QN-SPSA (blue solid line) and QN-CSPSA (red solid line). The black dashed line indicates the exact value of the ground state energy $E_0 = -6$. The shaded area represents the standard deviation (top) and the interquartile range (bottom). Statistical indicators are calculated on a sample of 10^4 repetitions of each optimization method.

After applying the GRAPE method for the evolution of the system, the final state is

$$|\tilde{\psi}_f\rangle = \prod_{i=1}^{M-1} e^{-\frac{i}{2}\theta_i \sigma_x} |\psi_0\rangle \quad (55)$$

where $|\psi_0\rangle$ is an initial single-qubit state and $\theta_i = u(t_{i+1}) - u(t_i)$ is the control parameter.

In the two-qubit case, the Bell state $|\psi_f\rangle = (|00\rangle + |11\rangle)/\sqrt{2}$ was chosen as the target state. We use the two-qubit Hamiltonian given by

$$H(t) = \sigma_x^{(1)} + u\sigma_+^{(1)}\sigma_-^{(2)} + u^*\sigma_-^{(1)}\sigma_+^{(2)}, \quad (56)$$

which can be physically realized on superconducting circuits [115]. After applying the GRAPE method for the evolution of the system, the final state is

$$|\tilde{\psi}_f\rangle = \prod_{i=1}^{M-1} e^{-i(\theta_i \sigma_+^{(1)}\sigma_-^{(2)} + \theta^* \sigma_-^{(1)}\sigma_+^{(2)})} |\psi_0\rangle \quad (57)$$

where $|\psi_0\rangle$ is a two-qubit initial state and $\theta_i = u(t_{i+1}) - u(t_i)$ is the control parameter.

The results of implementing GRAPE with the six different optimization algorithms in the single and two-qubit cases are shown in Figs. 4 and 5, respectively, where we display the value of the mean (upper row) and median (lower row) infidelity as a function of the number of measurements (evaluations of the objective function). The figures also display the variance and the interquartile range as shaded

areas. The first column contains the results obtained by SPSA (blue solid line) and CSPSA (red solid line). The second column contains the results obtained by 2SPSA (blue solid line) and 2CSPSA (red solid line). The third column contains the results obtained by QN-SPSA (blue solid line) and QN-CSPSA (red solid line). The mean, median, variance and interquartile range are estimated considering a sample of 10^4 estimates, which are generated considering uniformly distributed initial states $|\psi_0\rangle$. The values of the infidelity are obtained simulating a measurement process with a sample size of 2^{13} . In the single-qubit case, the GRAPE method considered $M = 15$. In the two-qubit case, the GRAPE method considered $M = 25$.

Figure 4 shows that the algorithms converge, reaching asymptotic regime before 500 measurements. For both the mean and the median, the first-order algorithms achieve the lowest infidelity values, while the natural gradient methods obtain the highest. The first-order algorithms present a much steeper decay than the others, entering in asymptotic regime after a small number of measurements. The variance is not noticeable in any of the algorithms, while the interquartile ranges are tighter for the first-order methods. Thus, the best performing algorithm is first-order CSPSA with standard gains, noting that almost 50% of the best CSPSA realizations are better than 75% of the worst realizations of all other methods. In particular, approximately 75% of the best first-order CSPSA realizations are better than 75% of the worst realizations of the complex natural gradient. Finally, we mention that within each type of method, it is the complex algorithms that achieve the best performance.

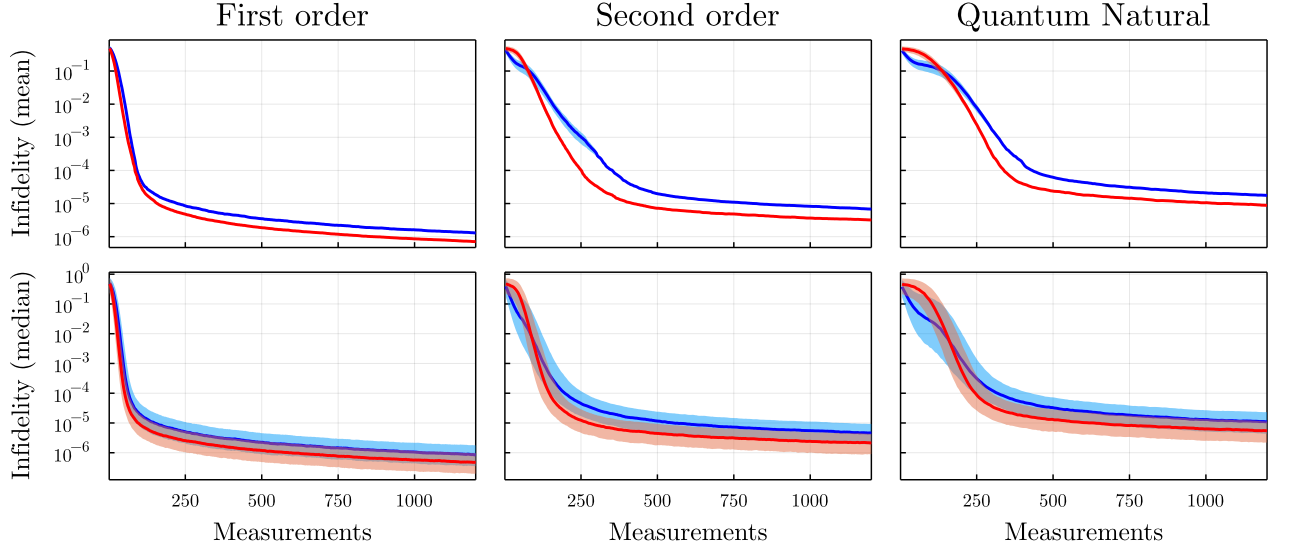


FIG. 4: The mean (top) and median (bottom) of the infidelity estimate as a function of the number of measurements obtained by performing quantum control by means GRAPE on a single qubit to generate the state $|\psi_f\rangle = |0\rangle$. From left to right, the columns show SPSA (blue solid line) and CSPSA (red solid line), 2SPSA (blue solid line) and 2CSPSA (red solid line), QN-SPSA (blue solid line) and QN-CSPSA (red solid line). Shaded areas represent variance (top) and interquartile range (bottom). First-order methods use the asymptotic gain coefficients, while the other methods use the standard gain coefficients. GRAPE uses $M = 15$ time intervals. Measurements of the infidelity are simulated with $N = 2^{13}$ shots. Statistical indicators are generated on a sample of 10^4 repetitions of each optimization method.

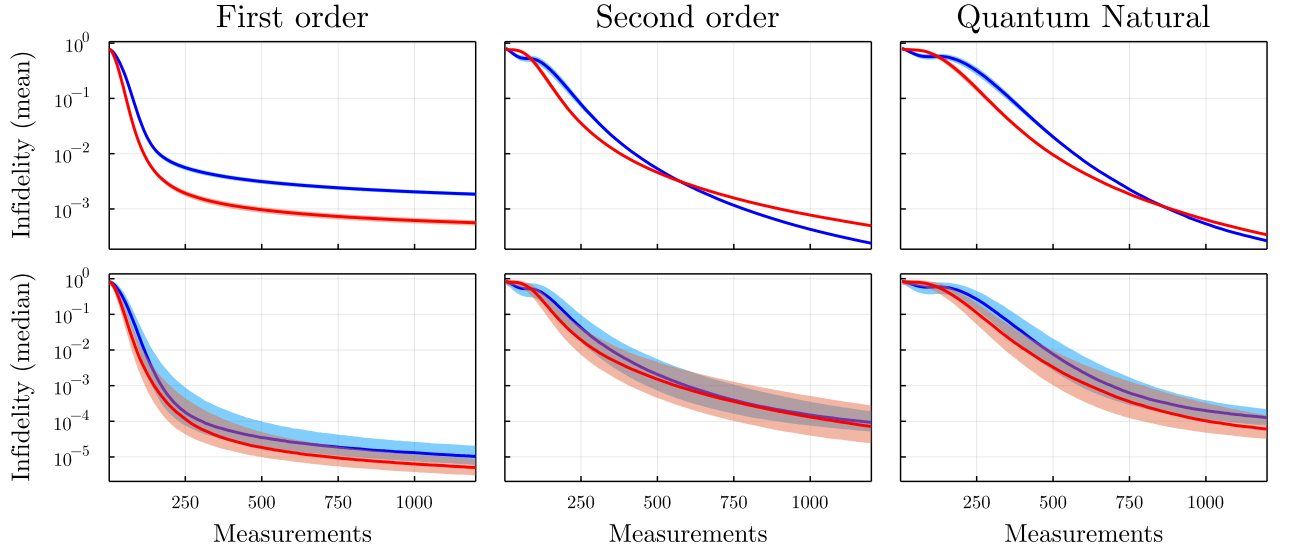


FIG. 5: The mean (top) and median (bottom) of the infidelity estimate as a function of the number of measurements obtained by performing quantum control by means GRAPE on two qubits to generate the state $|\psi_f\rangle = (|00\rangle + |11\rangle)/\sqrt{2}$. From left to right, the columns show SPSA (blue solid line) and CSPSA (red solid line), 2SPSA (blue solid line) and 2CSPSA (red solid line), QN-SPSA (blue solid line) and QN-CSPSA (red solid line). Shaded areas represent variance (top) and interquartile range (bottom). First-order methods use the asymptotic gain coefficients, while the other methods use the standard gain coefficients. GRAPE uses $M = 25$ time intervals. Measurements of the infidelity are simulated with $N = 2^{13}$ shots. Statistical indicators are generated on a sample of 10^4 repetitions of each optimization method.

Figure 5 shows that the methods converge and only the first-order algorithms start an asymptotic regime. Looking at the mean, we notice that the second-order and natural gradient algorithms obtain similar infidelity values. These values are lower than those obtained by means of the first-order methods. If we consider the median, the first-order algorithms obtain lower infidelity values, moving one order ahead of their competitors. The variance of the second-order and natural gradient methods decreases as the number of measurements increases, which is not the case for the first-order methods. The interquartile ranges are similar for all methods except first-order SPSA, which has twice the width of the interquartile range of the other algorithms. In the case of first-order algorithms, the difference between the mean and median convergence indicates the presence of realizations that converge at a lower rate. Thus, the best method for this problem would be first-order CSPSA with standard gains, noting that almost 75% of the best CSPSA realizations are better than 75% of the worst realizations of all other methods.

As is clear from the above analysis, the CSPSA algorithm with standard gains provides an advantage over SPSA, 2SPSA, 2CSPSA, QN-SPSA, and QN-CSPSA algorithms.

C. Quantum state estimation

Born's rule endows quantum mechanics with predictive power. According to this rule, the probability p_k of obtaining a result k in an experiment described by a POVM $\{E_k\}$ when the quantum system is described by a quantum state ρ is given by the Hilbert-Schmidt inner product $p_k = \text{Tr}(\rho E_k)$. Therefore, the comparison between theoretical predictions and experimental results requires an accurate characterization of the quantum state ρ and of the experiment through the POVM $\{E_k\}$. This leads to the problem of estimating quantum states and processes. For this purpose, several quantum state estimation methods have been designed, most of them based on the post-processing of experimental data acquired through the measurement of a fixed informationally complete POVM. Adaptive measurements have also been used to design quantum state estimation methods. Today, methods for estimating quantum states are an important tool for both quantum communications and quantum computing and have been used for the characterization of single-photon and continuous variable states [116–120], cavity fields [121], atomic ensembles [122–124], trapped ions [125, 126], optical detectors [127–129] and for quantum key distribution [130].

Recently, the estimation of pure states of finite dimension has been based on the variational characterization of a pure state [17]. According to this method, called self-guided quantum tomography (SGQT), the unknown state is considered the minimizer of infidelity $I(|\psi\rangle, |\phi\rangle) = 1 - |\langle\psi|\phi\rangle|^2$, that is,

$$|\psi\rangle = \arg \left(\min_{|\phi\rangle \in \mathcal{H}} I(|\psi\rangle, |\phi\rangle) \right). \quad (58)$$

This suggests the use of optimization algorithms to minimize the fidelity and estimate the unknown state $|\psi\rangle$. Gradient-based optimization is ruled out since it is not known how to

measure the gradient of the infidelity, with respect to the parameters entering in the state $|\phi\rangle$. However, the fidelity can be measured by projecting the unknown state onto any basis containing the state $|\phi\rangle$. In this scenario, the optimization methods introduced in the previous section can be used to experimentally implement the minimization of infidelity according to SGQT. The usage of SPSA was initially proposed in the original SGQT algorithm. Thereafter, CSPSA was introduced and applied to the estimation of pure quantum states obtaining an improvement in the convergence rate and less dispersion in the sample of estimates. Afterward, CSPSA was combined with maximum likelihood estimation to achieve an estimation accuracy close to the Gill-Massar lower bound, which is the best achievable estimation accuracy for pure states. The estimation of pure states via SPSA and CSPSA has been already experimentally demonstrated [18].

Figures 6, 7 and 8 display the mean (upper row) and median (lower row) infidelity as a function of the number of measurements (of infidelity) obtained when implementing the estimation of pure states of one, two and three qubits via SGQT. The first column contains the results obtained by SPSA (blue solid line) and CSPSA (red solid line). The second column contains the results obtained by 2SPSA (blue solid line) and 2CSPSA (red solid line). The third column contains the results obtained by QN-SPSA (blue solid line) and QN-CSPSA (red solid line). The figures also display the variance and the interquartile range as shaded areas. Mean, median, variance and interquartile range are calculated on a sample of 10^4 Haar-uniform distributed pairs of unknown state and initial guess state. Measurements of the infidelity are simulated with a binomial distribution with $N = 2^{13}$ shots. The simulations are executed using both sets of gains coefficients (standard and asymptotic), but choosing only the best performer for each method.

Figures 6, 7 and 8 exhibit a very similar behavior. The values of the mean and median are close and variance and interquartile range are very narrow, which shows the absence of outliers in the generated samples. Typically, all optimization algorithms are characterized by a sharp decrease of the infidelity followed by an approximately linear asymptotic regime. In the first regime, complex and real algorithms achieve a very similar performance. In the asymptotic regime the optimization algorithms for the field of the complex numbers outperform their real counterpart. Also in this regime and for 2 and 3 qubits, the second-order methods achieve a performance that is marginally better than natural-gradient methods. In the three studied cases the CSPSA algorithm provides the best results exhibiting the highest convergence rate and an interquartile range that is below all other interquartile ranges.

While optimizing a function, it may be possible that no a priori information about the Hessian matrix is available, either because of its high complexity or because it can not easily be obtained neither analytically nor numerically. For such cases, it would be desired that the second-order methods, that rely on approximating the Hessian matrix were still useful, in the case that unknown singularities are present. The geometry of the problem of pure state estimation is not recommended as the gradient vanishes as it gets closer to the optimum, so

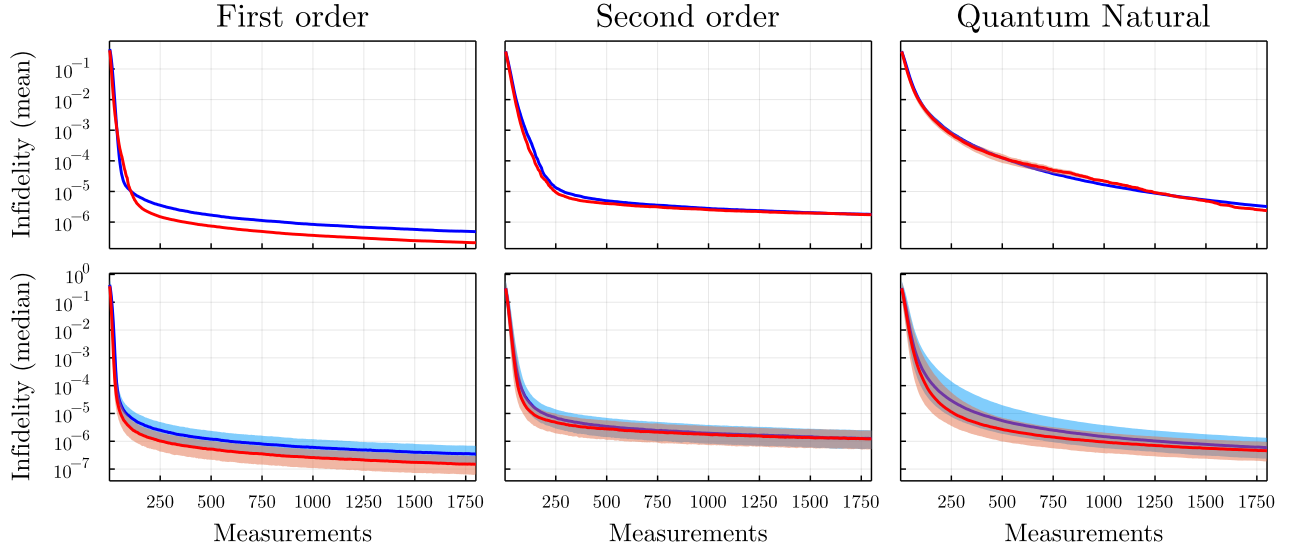


FIG. 6: The mean (top) and median (bottom) of the infidelity estimates as a function of the number of measurements obtained by using SGQT to estimate single-qubit states. From left to right, the columns show SPSA (blue solid line) and CSPSA (red solid line), 2SPSA (blue solid line) and 2CSPSA (red solid line), QN-SPSA (blue solid line) and QN-CSPSA (red solid line). Shaded areas represent variance (top) and interquartile range (bottom). The second-order methods use the standard gain coefficients, while the other methods use the asymptotic gain coefficients. Statistical indicators are calculated from a sample of 10^4 Haar-uniform distributed pairs of unknown state and initial guess state. Measurements of the infidelity are simulated with a binomial distribution with $N = 2^{13}$ shots.

in principle a second-order optimization should provide no advantage, or even difficult convergence and lower the precision. Nonetheless, the numerical simulations indicate that these methods, although are about one order of magnitude worse, still present a good enough convergence rate, with a small dispersion. By construction, the regularization imposed on the Hessian estimation explain this phenomena, making them converge to the first-order methods for multiple iterations with almost vanishing Hessian.

IV. CONCLUSIONS

In this paper, we presented a comprehensive comparison of different stochastic optimization methods applied to real-valued functions of complex variables. We started by reviewing the theory of the SPSA algorithm and two of its variants: 2SPSA and QN-SPSA. These three methods use a simultaneous perturbation stochastic approximation of the gradient of the objective function to optimize it. SPSA is a first-order algorithm while 2SPSA is of second-order. QN-SPSA is a first-order algorithm that preconditions considering a metric natural for the problem at hand. We also reviewed the CSPSA algorithm, which optimizes real functions of complex variables without resorting to the real and imaginary parts of complex variables. This is a more natural approach in the field of quantum mechanics, where most functions have complex arguments. Using CSPSA as starting point we developed two new optimization methods: 2CSPSA and QN-CSPSA, which are the complex field formulations of their real counterparts.

All the optimization methods here presented have the property that the number of evaluations (or measurements) of the objective function does not depend on the dimension of the optimization problem. This is an important advantage when the number of parameters our function depends on is large. The number of evaluations of the objective function is constant at each iteration but different for each method. SPSA and CSPSA use 2 evaluations of the objective function per iteration. 2SPSA and 2CSPSA use 4 evaluations of the objective function, since they are second-order methods. Finally, QN-SPSA and QN-CSPSA use 2 evaluations of the objective function plus the calculation of an approximation of a metric. If the metric is the Fubini-Study metric tensor, then the approximation is calculated by evaluating the infidelity with respect to 4 different pure states.

To assess the performance of the optimization methods we compare them in three important applications in quantum computing: variational quantum eigensolver, quantum control, and quantum state estimation. These three applications have their own objective function that needs to be measured in a quantum device and iteratively optimized to obtain a solution. Since current quantum devices are small, noisy and each measurement shot is expensive, we analyze the performance as a function of the corresponding quantum resource, for instance the number of total measurements or circuits.

Our simulations show several interesting results. In general, complex optimization methods achieve a higher or equal convergence rate than real optimization methods. The exceptions are the few cases where, after a certain number of iterations, the real optimization methods achieve better performance than

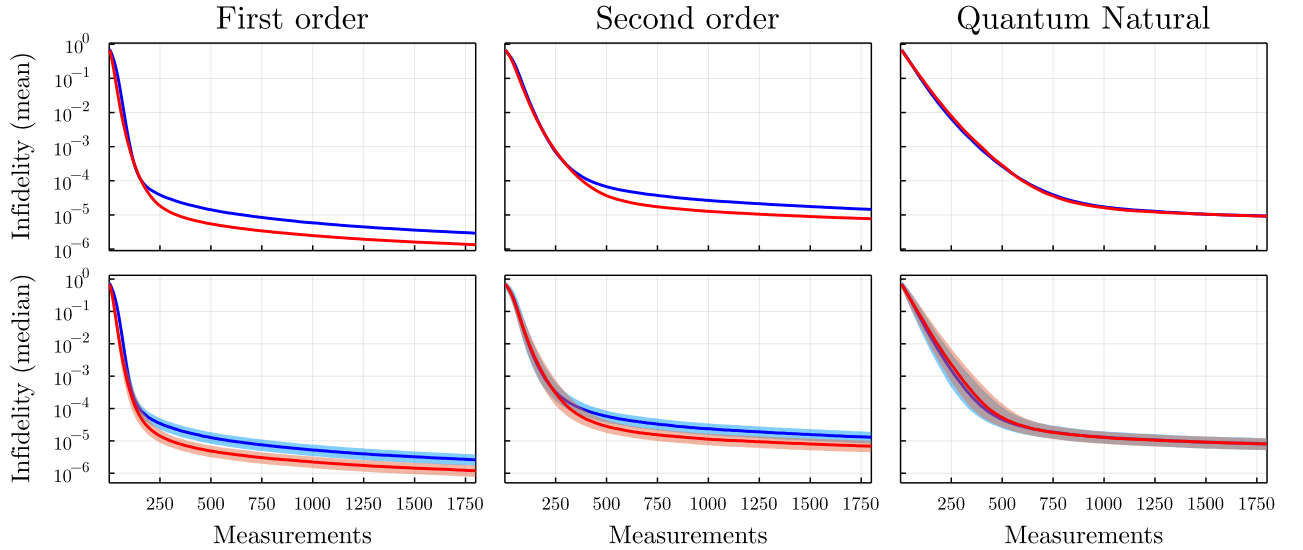


FIG. 7: The mean (top) and median (bottom) of the infidelity estimates as a function of the number of measurements obtained by using SGQT to estimate two-qubit states. From left to right, the columns show SPSA (blue solid line) and CSPSA (red solid line), 2SPSA (blue solid line) and 2CSPSA (red solid line), QN-SPSA (blue solid line) and QN-CSPSA (red solid line). Shaded areas represent variance (top) and interquartile range (bottom). The first-order methods use the asymptotic gain coefficients, while the other methods use the standard gain coefficients. Statistical indicators are calculated from a sample of 10^4 Haar-uniform distributed pairs of unknown state and initial guess state. Measurements of the infidelity are simulated with a binomial distribution with $N = 2^{13}$ shots.

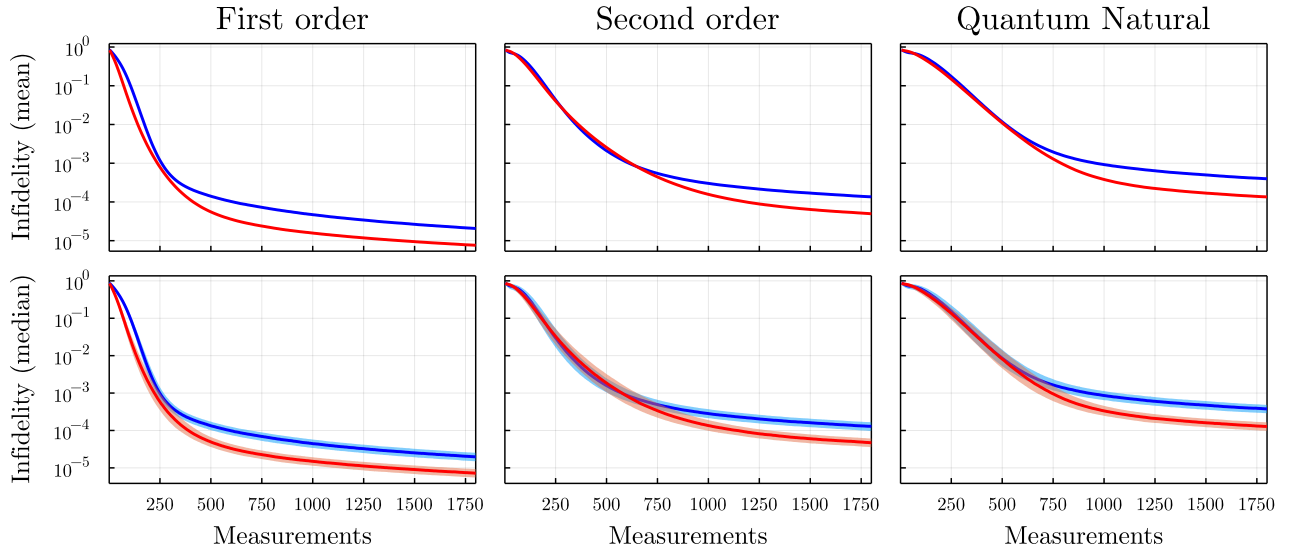


FIG. 8: The mean (top) and median (bottom) of the infidelity estimates as a function of the number of measurements obtained by using SGQT to estimate three-qubit states. From left to right, the columns show SPSA (blue solid line) and CSPSA (red solid line), 2SPSA (blue solid line) and 2CSPSA (red solid line), QN-SPSA (blue solid line) and QN-CSPSA (red solid line). Shaded areas represent variance (top) and interquartile range (bottom). The first-order methods use the asymptotic gain coefficients, while the other methods use the standard gain coefficients. Statistical indicators are calculated from a sample of 10^4 Haar-uniform distributed pairs of unknown state and initial guess state. Measurements of the infidelity are simulated with a binomial distribution with $N = 2^{13}$ shots.

the complex optimization methods, that is, the evolution of the objective function presents a crossover point. In the three

applications studied, CSPSA achieves better mean and median convergence than SPSA and narrower standard deviation

and interquartile range. Second-order methods, 2CSPSA and 2SPSA, lead to mixed results. These achieve a clear performance improvement over the first-order methods in the application to the variational quantum eigensolver. Unlike the first-order methods, 2CSPSA and 2SPSA show mean and median convergence, although mean convergence is slower than median convergence. Also, both second-order algorithms have a very similar behavior of the ground-state energy estimate as function of the number of circuits, standard deviation, and interquartile range. 2CSPSA and 2SPSA exhibit median convergence towards the true ground energy value of $E_0 = -6$ at approximately 5000 circuits, where SPSA and CSPSA reach a median ground-state energy estimate that is close to zero. CSPSA shows median convergence after approximately 17500 circuits. Thus, 2CSPSA and 2SPSA provide a large saving of resources and improved statistic with respect to the first-order methods. The application of the second-order methods to quantum control of quantum states shows an adverse result. In this case, 2CSPSA and 2SPSA are outperformed by the first-order methods. An analogous result arises in the case of quantum state estimation. Quantum natural gradient methods are expected to reach a performance better than first-order methods while using less resources than second-order methods. In the case of the variational quantum eigensolver, QN-CSPSA and QN-SPSA exhibit an identical median convergence while mean convergence is not achieved. The median convergence is almost identical to that provided by the second-order methods, thus outperforming the first-order methods. However, the variability exhibited by QN-CSPSA and QN-SPSA is much higher than that of 2CSPSA and 2SPSA. Thus, a single realization of QN-CSPSA and QN-SPSA leads with high probability to a ground-state energy estimate far from the true value. The application of QN-CSPSA and QN-SPSA to quantum control and quantum state estimation leads to results very similar to those obtained by the second-order methods, but not better than the first-order methods.

The stochastic optimization methods studied here are defined through a set of gain parameters, whose values specify the gain coefficients. These in turn control the step size and magnitude of the approximation of the gradient. In this way, the gain parameters play the role of hyper-parameters that allow controlling the rate of convergence of the algorithms. In

principle, it is conceivable to find gain parameters that lead to the best mean rate of convergence. This is, however, an expensive optimization problem whose solution might even depend on the optimizer of the objective function. Therefore, it is usual to resort to gain parameters that have proven to be good enough in practice. We have resorted to the standard gain parameters, which lead to a fast convergence in the regime of a small number of iterations, and to the asymptotic gain parameters, which lead to a fast convergence in the regime of a large number of iterations. Let us note that a change in the gain parameters does not only affects the mean and median convergence but also variance and interquartile range. According to the results of our study and taking into account that algorithms currently run for a small number of iterations, we recommend using first-order algorithms with standard gain parameters, and second-order and quantum natural gradient algorithms with asymptotic gain parameters.

In our comparative study we have considered a small number of qubits. This is mainly because the gradient of the objective functions decreases exponentially with increasing number of qubits. Therefore, for a larger number of qubits, the optimization algorithms face a very adverse scenario, where adequate techniques have not yet been developed. However, for a small number of qubits, the algorithms studied here can be experimentally implemented in the current generation of quantum processors and consequently test our results.

ACKNOWLEDGMENTS

This work was supported by ANID – Millennium Science Initiative Program – ICN17_012. J.A.G. was supported by ANID Chile, National Doctoral Degree Scholarship No. 21202616. L.P. was supported by ANID-PFCHA/DOCTORADO-BECAS-CHILE/2019-72200275, the Spanish project PGC2018-094792-B-I00 (MCIU/AEI/FEDER, UE), and CAM/FEDER Project No. S2018/TCS-4342 (QUITEMAD-CM). M.M. was supported by ANID-PFCHA/DOCTORADO-NACIONAL/2019-21190958. L.Z. was supported by ANID-PFCHA/DOCTORADO-NACIONAL/2018-21181021. A.D. was supported by FONDECYT Grant 1180558.

[1] J. Preskill, *Quantum* **2**, 79 (2018).

[2] N. Moll, P. Barkoutsos, L. S. Bishop, J. M. Chow, A. Cross, D. J. Egger, S. Filipp, A. Fuhrer, J. M. Gambetta, M. Ganzhorn, A. Kandala, A. Mezzacapo, P. Müller, W. Riess, G. Salis, *et al.*, *Quantum Science and Technology* **3**, 030503 (2018).

[3] J. R. McClean, J. Romero, R. Babbush, and A. Aspuru-Guzik, *New Journal of Physics* **18**, 023023 (2016).

[4] K. Bharti, A. Cervera-Lierta, T. H. Kyaw, T. Haug, S. Alperin-Lea, A. Anand, M. Degroote, H. Heimonen, J. S. Kottmann, T. Menke, W.-K. Mok, S. Sim, L.-C. Kwek, and A. Aspuru-Guzik, *Rev. Mod. Phys.* **94**, 015004 (2022).

[5] J. Tilly, H. Chen, S. Cao, D. Picozzi, K. Setia, Y. Li, E. Grant, L. Wossnig, I. Runger, G. H. Booth, and J. Tennyson, The variational quantum eigensolver: a review of methods and best practices (2021), [arXiv:2111.05176](https://arxiv.org/abs/2111.05176).

[6] B. P. Lanyon, J. D. Whitfield, G. G. Gillett, M. E. Goggin, M. P. Almeida, I. Kassal, J. D. Biamonte, M. Mohseni, B. J. Powell, M. Barbieri, A. Aspuru-Guzik, and A. G. White, *Nature Chemistry* **2**, 106 (2010).

[7] C. Hempel, C. Maier, J. Romero, J. McClean, T. Monz, H. Shen, P. Jurcevic, B. P. Lanyon, P. Love, R. Babbush, A. Aspuru-Guzik, R. Blatt, and C. F. Roos, *Phys. Rev. X* **8**, 031022 (2018).

[8] Y. Nam, J.-S. Chen, N. C. Pisenti, K. Wright, C. Delaney, D. Maslov, K. R. Brown, S. Allen, J. M. Amini, J. Apisdorf, K. M. Beck, A. Blinov, V. Chaplin, M. Chmielewski, C. Collins, *et al.*, *npj Quantum Information* **6**, 33 (2020).

[9] C. Ferrie and O. Moussa, *Phys. Rev. A* **91**, 052306 (2015).

[10] D. Lu, K. Li, J. Li, H. Katiyar, A. J. Park, G. Feng, T. Xin, H. Li, G. Long, A. Brodutch, J. Baugh, B. Zeng, and R. Laflamme, *npj Quantum Information* **3**, 45 (2017).

[11] D. J. Egger and F. K. Wilhelm, *Phys. Rev. Lett.* **112**, 240503 (2014).

[12] X. Yuan, S. Endo, Q. Zhao, Y. Li, and S. C. Benjamin, *Quantum* **3**, 191 (2019).

[13] S. Endo, J. Sun, Y. Li, S. C. Benjamin, and X. Yuan, *Phys. Rev. Lett.* **125**, 010501 (2020).

[14] X. Wang, Z. Song, and Y. Wang, *Quantum* **5**, 483 (2021).

[15] K. Wang, Z. Song, X. Zhao, Z. Wang, and X. Wang, Detecting and quantifying entanglement on near-term quantum devices (2020), [arXiv:2012.14311](https://arxiv.org/abs/2012.14311).

[16] A. D. Muñoz-Moller, L. Pereira, L. Zambrano, J. Cortés-Vega, and A. Delgado, Variational determination of multi-qubit geometrical entanglement in NISQ computers (2021), [arXiv:2110.03709](https://arxiv.org/abs/2110.03709).

[17] C. Ferrie, *Phys. Rev. Lett.* **113**, 190404 (2014).

[18] R. J. Chapman, C. Ferrie, and A. Peruzzo, *Phys. Rev. Lett.* **117**, 040402 (2016).

[19] A. Utreras-Alarcón, M. Rivera-Tapia, S. Niklitschek, and A. Delgado, *Scientific Reports* **9**, 16143 (2019).

[20] L. Zambrano, L. Pereira, S. Niklitschek, and A. Delgado, *Sci. Rep.* **10**, 12781 (2020).

[21] M. Rambach, M. Qaryan, M. Kewming, C. Ferrie, A. G. White, and J. Romero, *Phys. Rev. Lett.* **126**, 100402 (2021).

[22] J. Biamonte, P. Wittek, N. Pancotti, P. Rebentrost, N. Wiebe, and S. Lloyd, *Nature* **549**, 195 (2017).

[23] M. Benedetti, E. Grant, L. Wossnig, and S. Severini, *New Journal of Physics* **21**, 043023 (2019).

[24] A. Patterson, H. Chen, L. Wossnig, S. Severini, D. Browne, and I. Rungger, *Phys. Rev. Research* **3**, 013063 (2021).

[25] H. Chen, L. Wossnig, S. Severini, H. Neven, and M. Mohseni, *Quantum Machine Intelligence* **3**, 1 (2020).

[26] D. Concha, L. Pereira, L. Zambrano, and A. Delgado, *Training quantum measurement devices to discriminate unknown non-orthogonal quantum states* (2021).

[27] X. Xu, S. C. Benjamin, and X. Yuan, *Phys. Rev. Applied* **15**, 034068 (2021).

[28] E. Farhi, J. Goldstone, and S. Gutmann, A quantum approximate optimization algorithm (2014), [arXiv:1411.4028](https://arxiv.org/abs/1411.4028).

[29] L. Zhou, S.-T. Wang, S. Choi, H. Pichler, and M. D. Lukin, *Phys. Rev. X* **10**, 021067 (2020).

[30] M. P. Harrigan, K. J. Sung, M. Neeley, K. J. Satzinger, F. Arute, K. Arya, J. Atalaya, J. C. Bardin, R. Barends, S. Boixo, M. Broughton, B. B. Buckley, D. A. Buell, B. Burkett, N. Bushnell, *et al.*, *Nature Physics* **17**, 332 (2021).

[31] K. Kubo, Y. O. Nakagawa, S. Endo, and S. Nagayama, *Phys. Rev. A* **103**, 052425 (2021).

[32] M. Lubasch, J. Joo, P. Moinier, M. Kiffner, and D. Jaksch, *Phys. Rev. A* **101**, 010301 (2020).

[33] P. García-Molina, J. Rodríguez-Mediavilla, and J. J. García-Ripoll, *Phys. Rev. A* **105**, 012433 (2022).

[34] D. Herman, C. Googin, X. Liu, A. Galda, I. Safro, Y. Sun, M. Pistoia, and Y. Alexeev, *A survey of quantum computing for finance* (2022), [arXiv:2201.02773](https://arxiv.org/abs/2201.02773).

[35] J. R. McClean, S. Boixo, V. N. Smelyanskiy, R. Babbush, and H. Neven, *Nature Communications* **9**, 4812 (2018).

[36] A. Arrasmith, M. Cerezo, P. Czarnik, L. Cincio, and P. J. Coles, *Quantum* **5**, 558 (2021).

[37] K. J. Sung, J. Yao, M. P. Harrigan, N. C. Rubin, Z. Jiang, L. Lin, R. Babbush, and J. R. McClean, *Quantum Science and Technology* **5**, 044008 (2020).

[38] O. Lockwood, *An empirical review of optimization techniques for quantum variational circuits* (2022), [arXiv:2202.01389](https://arxiv.org/abs/2202.01389).

[39] W. Lavrijsen, A. Tudor, J. Muller, C. Iancu, and W. de Jong, in *2020 IEEE International Conference on Quantum Computing and Engineering (QCE)* (IEEE, 2020) pp. 267–277.

[40] X. Bonet-Monroig, H. Wang, D. Vermetten, B. Senjean, C. Moussa, T. Bäck, V. Dunjko, and T. E. O'Brien, Performance comparison of optimization methods on variational quantum algorithms (2021), [arXiv:2111.13454](https://arxiv.org/abs/2111.13454).

[41] D. Saad, ed., *On-Line Learning in Neural Networks* (Cambridge University Press, 1999).

[42] J. Duchi, E. Hazan, and Y. Singer, *J. Mach. Learn. Res.* **12**, 2121–2159 (2011).

[43] T. Tieleman, G. Hinton, *et al.*, COURSERA: Neural networks for machine learning **4**, 26 (2012).

[44] D. P. Kingma and J. Ba, *Adam: A method for stochastic optimization* (2014), [arXiv:1412.6980](https://arxiv.org/abs/1412.6980).

[45] T. Dozat, *Incorporating nesterov momentum into adam* (2016).

[46] S. J. Reddi, S. Kale, and S. Kumar, *On the convergence of adam and beyond* (2019), [arXiv:1904.09237](https://arxiv.org/abs/1904.09237).

[47] J. A. Nelder and R. Mead, *The Computer Journal* **7**, 308 (1965).

[48] M. J. D. Powell, *The Computer Journal* **7**, 155 (1964).

[49] S. G. Nash, *SIAM Journal on Numerical Analysis* **21**, 770 (1984).

[50] D. Kraft, *A software package for sequential quadratic programming*, Deutsche Forschungs- und Versuchsanstalt für Luft- und Raumfahrt Köln: Forschungsbericht (Wiss. Berichtswesen d. DFVLR, 1988).

[51] R. Fletcher and C. M. Reeves, *The Computer Journal* **7**, 149 (1964).

[52] M. J. D. Powell, in *Advances in Optimization and Numerical Analysis* (Springer Netherlands, 1994) pp. 51–67.

[53] R. H. Byrd, P. Lu, J. Nocedal, and C. Zhu, *SIAM Journal on Scientific Computing* **16**, 1190 (1995).

[54] M. Lalee, J. Nocedal, and T. Plantenga, *SIAM Journal on Optimization* **8**, 682 (1998).

[55] S. W. Jorge Nocedal, *Numerical Optimization* (Springer New York, 2006).

[56] P. Virtanen, R. Gommers, T. E. Oliphant, M. Haberland, T. Reddy, D. Cournapeau, E. Burovski, P. Peterson, W. Weckesser, J. Bright, S. J. van der Walt, M. Brett, J. Wilson, K. J. Millman, N. Mayorov, *et al.*, *Nature Methods* **17**, 261 (2020).

[57] H. J. Kushner and D. S. Clark, *Stochastic Approximation Methods for Constrained and Unconstrained Systems*, Vol. 26 (Springer New York, 1978).

[58] H. J. Kushner and G. G. Yin, *Stochastic Approximation Algorithms and Applications* (Springer New York, 1997).

[59] A. E. Albert and L. A. Gardner, *Stochastic Approximation and NonLinear Regression* (The MIT Press, 2003).

[60] J. Spall, *IEEE Transactions on Neural Networks* **18** (2007).

[61] S. Bhatnagar, H. Prasad, and L. Prashanth, *Stochastic Recursive Algorithms for Optimization*, Vol. 434 (Springer London, 2013).

[62] J. C. Spall, in *1987 American Control Conference* (1987) pp. 1161–1167.

[63] A. Kandala, A. Mezzacapo, K. Temme, M. Takita, M. Brink, J. M. Chow, and J. M. Gambetta, *Nature* **549**, 242 (2017).

[64] O. V. Borzenkova, G. I. Struchalin, A. S. Kardashin, V. V. Krasnikov, N. N. Skryabin, S. S. Straupe, S. P. Kulik, and J. D. Biamonte, *Applied Physics Letters* **118**, 144002 (2021).

[65] I. Hamamura and T. Imamichi, *npj Quantum Information* **6**, 56 (2020).

[66] F. Escudero, D. Fernández-Fernández, G. Jaumà, G. F. Peñas, and L. Pereira, *Hardware-efficient entangled measurements for variational quantum algorithms* (2022), arXiv:2202.06979.

[67] P. Díez-Valle, D. Porras, and J. J. García-Ripoll, *Phys. Rev. A* **104**, 062426 (2021).

[68] M. Benedetti, E. Lloyd, S. Sack, and M. Fiorentini, *Quantum Science and Technology* **4**, 043001 (2019).

[69] S. Mangini, F. Tacchino, D. Gerace, C. Macchiavello, and D. Bajoni, *Machine Learning: Science and Technology* **1**, 045008 (2020).

[70] G. Agliardi and E. Prati, *Quantum Reports* **4**, 75 (2022).

[71] Z. Hou, J.-F. Tang, C. Ferrie, G.-Y. Xiang, C.-F. Li, and G.-C. Guo, *Phys. Rev. A* **101**, 022317 (2020).

[72] J. Spall, *Automatic Control, IEEE Transactions on* **45**, 1839 (2000).

[73] C. Wang, *An overview of spsa: recent development and applications* (2020), arXiv:2012.06952.

[74] X. Zhu and J. C. Spall, *International Journal of Adaptive Control and Signal Processing* **16**, 397 (2002).

[75] J. Stokes, J. Izaac, N. Killoran, and G. Carleo, *Quantum* **4**, 269 (2020).

[76] S. Amari, *Neural Computation* **10**, 251 (1998).

[77] T. Liang, T. Poggio, A. Raklin, and J. Stokes, in *Proceedings of the Twenty-Second International Conference on Artificial Intelligence and Statistics*, Proceedings of Machine Learning Research, Vol. 89, edited by K. Chaudhuri and M. Sugiyama (PMLR, 2019) pp. 888–896.

[78] J. Gacon, C. Zoufal, G. Carleo, and S. Woerner, *Quantum* **5**, 567 (2021).

[79] H. Buhrman, R. Cleve, J. Watrous, and R. de Wolf, *Phys. Rev. Lett.* **87**, 167902 (2001).

[80] Q. Wang, Z. Zhang, K. Chen, J. Guan, W. Fang, and M. Ying, *Quantum algorithm for fidelity estimation* (2021), arXiv:2103.09076.

[81] P. Gokhale, O. Angiuli, Y. Ding, K. Gui, T. Tomesh, M. Suchara, M. Martonosi, and F. T. Chong, *Minimizing state preparations in variational quantum eigensolver by partitioning into commuting families* (2019), arXiv:1907.13623.

[82] S. Bravyi, J. M. Gambetta, A. Mezzacapo, and K. Temme, *Tapering off qubits to simulate fermionic hamiltonians* (2017), arXiv:1701.08213.

[83] N. Yamamoto, *On the natural gradient for variational quantum eigensolver* (2019), arXiv:1909.05074.

[84] D. Wierichs, C. Gogolin, and M. Kastoryano, *Phys. Rev. Research* **2**, 043246 (2020).

[85] B. van Straaten and B. Koczor, *PRX Quantum* **2**, 030324 (2021).

[86] W. Wirtinger, *Mathematische Annalen* **97**, 357 (1927).

[87] K. Kreutz-Delgado, *The complex gradient operator and the CR-calculus* (2009), arXiv:0906.4835 [math.OC].

[88] Y. Yao, P. Cusenot, R. A. Wolf, and F. M. Miatto, arXiv preprint arXiv:2106.13660 (2021).

[89] S. Zhang, Y. Xia, and J. Wang, *IEEE Transactions on Neural Networks and Learning Systems* **26**, 3227 (2015).

[90] A. Hirose, *Complex-Valued Neural Networks*, Vol. 400 (Springer Berlin Heidelberg, 2012).

[91] O. M. Smirnov and C. Tasse, *Monthly Notices of the Royal Astronomical Society* **449**, 2668 (2015).

[92] J. M. Arrazola, T. R. Bromley, J. Izaac, C. R. Myers, K. Brádler, and N. Killoran, *Quantum Science and Technology* **4**, 024004 (2019).

[93] N. Killoran, T. R. Bromley, J. M. Arrazola, M. Schuld, N. Quesada, and S. Lloyd, *Phys. Rev. Research* **1**, 033063 (2019).

[94] N. Khaneja, T. Reiss, C. Kehlet, T. Schulte-Herbrüggen, and S. J. Glaser, *Journal of Magnetic Resonance* **172**, 296 (2005).

[95] L. Sorber, M. V. Barel, and L. D. Lathauwer, *SIAM Journal on Optimization* **22**, 879 (2012).

[96] H. Robbins and S. Monro, *The Annals of Mathematical Statistics* **22**, 400 (1951).

[97] J. Kiefer and J. Wolfowitz, *The Annals of Mathematical Statistics* **23**, 462 (1952).

[98] Note that one could use a centered finite-difference scheme for approximating the Hessian from the gradient, but we choose a forward difference scheme, as presented by Spall [72], because it allows to reuse the measurements for the gradient, consequently reducing the total number of function evaluations from 6 to 4 per iteration.

[99] S. Amari and S. Douglas, in *Proceedings of the 1998 IEEE International Conference on Acoustics, Speech and Signal Processing, ICASSP '98 (Cat. No. 98CH36181)* (IEEE, 2002).

[100] G. Yan and H. Fan, *IEEE Transactions on Signal Processing* **48**, 553 (2000).

[101] M. Muñoz, L. Pereira, S. Niklitschek, and A. Delgado, *Complex field formulation of the quantum estimation theory* (2022), arXiv:2203.03064.

[102] W. Ritz, *Journal für die reine und angewandte Mathematik (Crelles Journal)* **135**, 1 (1909).

[103] J. Rayleigh, *Phil. Trans.* **161**, 75 (1870).

[104] A. Peruzzo, J. McClean, P. Shadbolt, M.-H. Yung, X.-Q. Zhou, P. J. Love, A. Aspuru-Guzik, and J. L. O'Brien, *Nature Communications* **5**, 4213 (2014).

[105] X.-Z. Luo, J.-G. Liu, P. Zhang, and L. Wang, arXiv preprint arXiv:1912.10877 (2019).

[106] M. Shapiro and P. Brumer, *Quantum Control of Molecular Processes* (Wiley-VCH Verlag GmbH & Co. KGaA, 2011).

[107] S. Chu, *Nature* **416**, 206 (2002).

[108] R. van Handel, J. K. Stockton, and H. Mabuchi, *Journal of Optics B: Quantum and Semiclassical Optics* **7**, S179 (2005).

[109] S. Lloyd, *Phys. Rev. A* **62**, 022108 (2000).

[110] J. Werschnik and E. K. U. Gross, *Journal of Physics B: Atomic, Molecular and Optical Physics* **40**, R175 (2007).

[111] D. Burgarth, P. Facchi, H. Nakazato, S. Pascazio, and K. Yuasa, *Quantum* **3**, 152 (2019).

[112] G. Quiroz, *Phys. Rev. A* **99**, 062306 (2019).

[113] B. B. Zhou, A. Baksic, H. Ribeiro, C. G. Yale, F. J. Herremans, P. C. Jerger, A. Auer, G. Burkard, A. A. Clerk, and D. D. Awschalom, *Nature Physics* **13**, 330 (2016).

[114] Z. Wu and H. Yang, *Phys. Rev. A* **72**, 012114 (2005).

[115] A. Blais, R.-S. Huang, A. Wallraff, S. M. Girvin, and R. J. Schoelkopf, *Phys. Rev. A* **69**, 062320 (2004).

[116] K. Laiho, M. Avenhaus, and C. Silberhorn, *New Journal of Physics* **14**, 105011 (2012).

[117] A. M. Brańczyk, D. H. Mahler, L. A. Rozema, A. Darabi, A. M. Steinberg, and D. F. V. James, *New Journal of Physics* **14**, 085003 (2012).

[118] C. R. Müller, B. Stoklasa, C. Peuntinger, C. Gabriel, J. Řeháček, Z. Hradil, A. B. Klimov, G. Leuchs, C. Marquardt, and L. L. Sánchez-Soto, *New Journal of Physics* **14**, 085002 (2012).

[119] A. Chiuri, L. Mazzola, M. Paternostro, and P. Mataloni, *New Journal of Physics* **14**, 085006 (2012).

[120] S. Wallentowitz, B. Seifert, and S. Godoy, *New Journal of Physics* **14**, 085007 (2012).

Physics **14**, 105019 (2012).

[121] C. Sayrin, I. Dotsenko, S. Gleyzes, M. Brune, J. M. Raimond, and S. Haroche, *New Journal of Physics* **14**, 115007 (2012).

[122] S. L. Christensen, J. B. Béguin, H. L. Sørensen, E. Bookjans, D. Oblak, J. H. Müller, J. Appel, and E. S. Polzik, *New Journal of Physics* **15**, 015002 (2013).

[123] R. R. de Castro, R. Cabrera, D. I. Bondar, and H. Rabitz, *New Journal of Physics* **15**, 025032 (2013).

[124] M. W. Mitchell, M. Koschorreck, M. Kubasik, M. Napolitano, and R. J. Sewell, *New Journal of Physics* **14**, 085021 (2012).

[125] M. Gută, T. Kypraios, and I. Dryden, *New Journal of Physics* **14**, 105002 (2012).

[126] H. Häffner, W. Hänsel, C. F. Roos, J. Benhelm, D. C. al kar, M. Chwalla, T. Körber, U. D. Rapol, M. Riebe, P. O. Schmidt, C. Becher, O. Gühne, W. Dür, and R. Blatt, *Nature* **438**, 643 (2005).

[127] L. Zhang, A. Datta, H. B. Coldenstrodt-Ronge, X.-M. Jin, J. Eisert, M. B. Plenio, and I. A. Walmsley, *New Journal of Physics* **14**, 115005 (2012).

[128] G. Brida, L. Ciavarella, I. P. Degiovanni, M. Genovese, L. Lolli, M. G. Mingolla, F. Piacentini, M. Rajteri, E. Taralli, and M. G. A. Paris, *New Journal of Physics* **14**, 085001 (2012).

[129] A. Anis and A. I. Lvovsky, *New Journal of Physics* **14**, 105021 (2012).

[130] S. Watanabe, R. Matsumoto, and T. Uyematsu, *Phys. Rev. A* **78**, 042316 (2008).

[131] M. Cerezo, A. Arrasmith, R. Babbush, S. C. Benjamin, S. Endo, K. Fujii, J. R. McClean, K. Mitarai, X. Yuan, L. Cincio, and P. J. Coles, *Nature Reviews Physics* **3**, 625 (2021).

[132] K. Bharti, A. Cervera-Lierta, T. H. Kyaw, T. Haug, S. Alperin-Lea, A. Anand, M. Degroote, H. Heimonen, J. S. Kottmann, T. Menke, W.-K. Mok, S. Sim, L.-C. Kwek, and A. Aspuru-Guzik, *Noisy intermediate-scale quantum NISQ algorithms* (2021), arXiv:2101.08448 [quant-ph].

[133] Z. Hradil, *Physical Review A* **55**, R1561 (1997).

[134] J. B. Altepeter, D. F. James, and P. G. Kwiat, in *Quantum State Estimation* (Springer Berlin Heidelberg, 2004) pp. 113–145.

[135] U. Leonhardt, H. Paul, and G. M. D’Ariano, *Physical Review A* **52**, 4899 (1995).

[136] R. T. Thew, K. Nemoto, A. G. White, and W. J. Munro, *Phys. Rev. A* **66**, 012303 (2002).

[137] J. M. Renes, R. Blume-Kohout, A. J. Scott, and C. M. Caves, *Journal of Mathematical Physics* **45**, 2171 (2004).

[138] D. Gross, Y.-K. Liu, S. T. Flammia, S. Becker, and J. Eisert, *Phys. Rev. Lett.* **105**, 150401 (2010).

[139] S. N. Filippov and V. I. Man’ko, *Physica Scripta* **T143**, 014010 (2011).

[140] H. Kushner and G. Yin, *Stochastic Approximation and Recursive Algorithms and Applications*, Vol. 35 (Springer-Verlag, 2003).

[141] L. Cincio, Y. Subaşı, A. T. Sornborger, and P. J. Coles, *New Journal of Physics* **20**, 113022 (2018).

[142] V. Havlíček, A. D. Córcoles, K. Temme, A. W. Harrow, A. Kandala, J. M. Chow, and J. M. Gambetta, *Nature* **567**, 209 (2019).